EXPERIMENTAL STUDY OF CRITICAL CASIMIR FORCES ON MICROPARTICLES IN CRITICAL BINARY LIQUID MIXTURES

A THESIS

SUBMITTED TO THE DEPARTMENT OF MATERIAL SCIENCE AND NANOTECHNOLOGY

AND THE GRADUATE SCHOOL OF ENGINEERING AND SCIENCE

OF BILKENT UNIVERSITY

IN PARTIAL FULFILLMENT OF THE REQUIREMENTS

FOR THE DEGREE OF

MASTER OF SCIENCE

By

Yazgan Tuna

August, 2014

I certify that I have read this thesis and that in my opinion it is fully adequate, in scope and in quality, as a thesis for the degree of Master of Science.

Asst. Prof. Dr. Giovanni Volpe (Advisor)

I certify that I have read this thesis and that in my opinion it is fully adequate, in scope and in quality, as a thesis for the degree of Master of Science.

Assoc. Prof. Dr. Mehmet Burçin Ünlü

I certify that I have read this thesis and that in my opinion it is fully adequate, in scope and in quality, as a thesis for the degree of Master of Science.

Asst. Prof. Dr. Ali Kemal Okyay

Approved for the Graduate School of Engineering and Science:

Prof. Dr. Levent Onural
Director of the Graduate School

ABSTRACT

EXPERIMENTAL STUDY OF CRITICAL CASIMIR FORCES ON MICROPARTICLES IN CRITICAL BINARY LIQUID MIXTURES

Yazgan Tuna
M.S. in Material Science and Nanotechnology
Supervisor: Asst. Prof. Dr. Giovanni Volpe
August, 2014

Long-ranged forces between mesoscopic objects emerge when a fluctuating field is confined. Analogously to the well known quantum-electro-dynamical (QED) Casimir forces, emerging between conducting objects due to the confinement of the vacuum electromagnetic fluctuations, critical Casimir forces emerge between objects due to confinement of the fluid density fluctuations. Here, we studied experimentally several novel aspects and applications of critical Casimir fluctuations in a critical mixture of walter-2,6-lutidine, which are a promising candidate to harness forces and interactions at mesoscopic and nanoscopic length-scales and promise to deliver results of both fundamental and applied interest. In particular, we studied the critical Casimir forces between multiple objects and multiple-body effects. We first extended the experimental study of critical Casimir forces in configurations different from the particle-wall system[1]. The forces acting between two particles in far from any surface and the third particle effect were explored. Then we employed multiple reconfigurable holographic optical tweezers (HOTs) which permit to optically trap several colloids and used a technique known as "digital video microscopy" (DVM) to track the particles' trajectories and the forces acting on the particles. We studied the critical Casimir force arising between two particles as a function of their distance and investigated how this is affected by the presence of a third neighboring particle.

Keywords: Critical Fluctuations, Critical Casimir Forces, Quantum-electro-dynamical Casimir Forces, Force Measurement, Optical Tweezers, Photonic Force Microscopy, Digital Video Microscopy.

ÖZET

İKİ BİLEŞENLİ SIVI KARIŞIMLARDA MİKROPARTİKÜLLER ÜZERİNDEKİ KRİTİK CASİMİR KUVVETİ ÜZERİNE DENEYSEL ÇALŞMA

Yazgan Tuna
Malzeme Bilimi ve Nanoteknoloji, Yüksek Lisans
Tez Yöneticisi: Asst. Prof. Dr. Giovanni Volpe
Ağustos, 2014

Dalgalanan bir ortam sınırlandığında, mesoskopik objeler arasında uzun menzilli kuvvetler açığa çıkar. İki iletken levha arasında vakum dalgalanmalarının sınırlanmasına bağlı olarak açığa çıkan Kuvantum Elektrodinamik(QED) Casimir kuvvetlerine analog olarak, kritik noktaya yakın bulunan kritik karışım içinde meydana gelen faz dalgalanmalarının sınırlanmasından dolayı da, sınırlayan objeler arasında kritik Casimir kuvvetleri ortaya çıkmaktadır. Burada, açığa çıkan kuvvetlerin incelenmesi, kullanılması, meso ve nano boyutlardaki etkileşimlerin incelenmesi için en uygun örnek olarak görünen su-2,6 lutidin kritik karışımı içinde oluşan kritik Casimir kuvvetlerini, deneysel olarak ve uygulamaları açısından çalıştık ve bu çalışmalar hem temel bilim hem de uygulama alanları açısından oldukça umut vericidir. Özellikle, burada birden fazla obje arasında oluşan kritik Casimir kuvvetlerini ve çoklu kütle etkilerini inceledik. Ayrıca, deneylerimizi parçacık-duvar etkileşiminin[1] ötesinde farklı dizilimlerle de genişlettik. İki ve üç parçacık arasındaki etkileşimi yüzeyden uzakta ölçüp kuvvetlerin davranışını inceledik. Bunun için de çoklu optik tuzaklar oluşturup parçacıkları yüzeyden yukarıya taşıdık ve Dijital Video Mikroskobu olarak bilinen yöntem ile parçacıkların yörüngelerini ve kuvvetlerin etkisini inceledik.

Anahtar sözcükler: Kritik salınımlar, kritik Casimir kuvvetleri, kuvantum elektrodinamik Casimir kuvvetleri, kuvvet ölçümleri, optik cımbız, fotonik kuvvet mikroskopisi, dijital video mikroskopisi.

Acknowledgement

I would like to express my deepest appreciation to my advisor Dr. Giovanni Volpe. Without his insightful guidance and persistent help, this dessertation would not have been possible. He always treated his student as collegaues and gave us the chance to follow our insticts in the lab. He never gave up being patiently supportive and inspired all of us to become honorable scientista like himself. I cannot thank enough to him for his kind help in both academic and personal matters. I feel extremely lucky to have the chance to work with such a briliant scientist and person. Thank you!

I am extremely thankful to Dr. Bülend Ortaç for his guidance, inpiring disscussions and countless help during my years in Bilkent. I am very glad to meet such a kind and successful person. Thank you!

I would also like to thank every single member of Soft-Matter Lab for creating such a good atmosphere to do research and for their friendship. I especially would like to thank my lab-mates Sathyanarayana Paladugu, K. P. Velu Sabareesh and Seyfullah Yılmaz for their enjoyable company and kind help. I also need to thank Dr. Agnese Callegari in particular, for her countless help with everthing.

I feel very lucky to have friends like Abdulsamet Akpınar, Kerem Emre Ercan, Emre Çağırıcı, M. Emin Öztük, Burak Gököz and Tamer Doğan. I especially would like to thank to my corporate partners, collegues and friends Özer Duman and Ahmet Burak Cunbul. And special thanks to Doğukan Bozkurt and İbrahim Örender for being more than friends to me since my childhood.

Finally, I would like to thank to my family; thank you my brothers Burak and Arda, my mother Birgül and my father Recep for always being there for me. Last but not least, thank you to my lovely wife Aylin for being always so considerate and supportive. Thank you!

Contents

List of Figures

List of Tables

Chapter 1

Introduction

Critical Casimir forces were first proposed 1978 by Fisher and de Gennes[6] in analogy to quantum-electro-dinamical (QED) Casimir forces[7]. QED Casimir forces arise when two conducting objects are brought in close proximity to one another because the vacuum fluctuations in the electromagnetic field between them create a pressure. Critical Casimir forces are their thermodynamic analog; (in this case, thermal fluctuations of a local order parameter) near a continuous phase transition can attract or repel nearby objects when they are in confinement[8]. Such thermal fluctuations in a condensed matter system typically occur on molecular (subnanometer) length-scales. However, approaching a critical point of a second-order phase transition, the fluctuations of the order parameter become relevant on much larger length-scales (ξ). The confinement of such fluctuations can induce forces between nearby objects. The first direct evidence for such forces was provided in 2008[1]: femtonewton forces were experimentally measured between a micrometer colloidal particle and a silica surface immersed in a water-2,6-lutidine mixture employing total internal reflection microscopy (TIRM); interestingly, both attractive and repulse forces were demonstrated. Since then, various studies have been performed to characterize the behavior of critical forces under various conditions; in particular, varying the boundary conditions[9] and the salt concentration in the mixture[10]. Also there have been various studies of the phase behavior of large aggregates of particles in

a critical mixture[11].

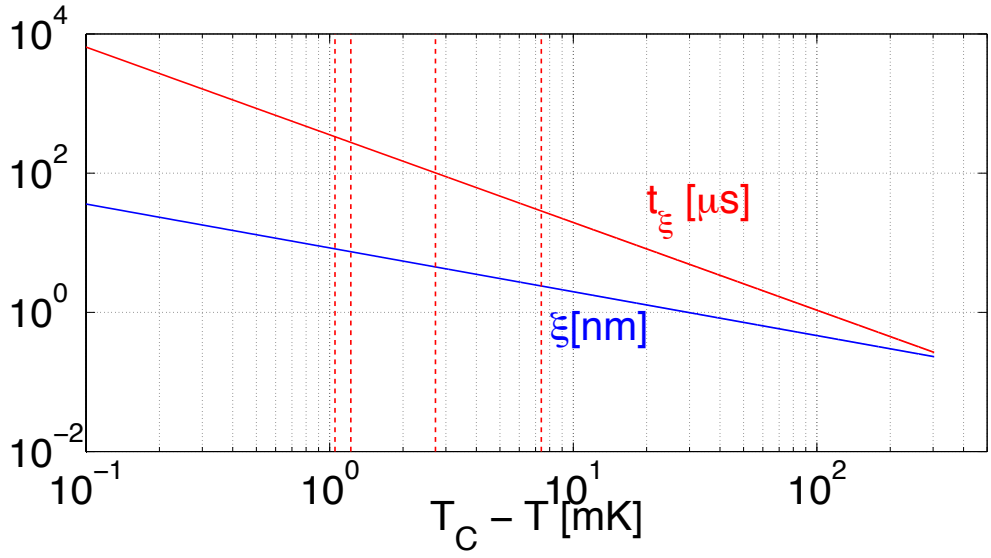

Figure 1.1: Dependence of the bulk correlation length ξ and of the bulk relaxation time t_ξ of the order parameter fluctuations in a water-2,6-lutidine mixture at critical concentration, as a function of the distance $T_c - T$ from the critical point. *The vertical dashed lines indicate the typical distances from the critical point explored in our experiments, which result in the range of correlation lengths indicated by the blue horizontal stripe. The corresponding expected range of relaxation times is indicated by the red stripe. The theoretical prediction $\tau_\xi \propto \xi^3$ for the specific relation in the case of the water-2,6-lutidine mixture is based on mode-coupling theory[2, 3].*

Here, we have investigated experimentally several novel aspects and applications of critical Casimir fluctuations, which are a promising candidate to harness forces and interactions at mesoscopic and nanoscopic length-scales and promise to deliver results of both fundamental and applied interest. In particular, we have studied critical Casimir forces arising in various configurations of multiple particles. In fact, before this study, the only configuration that had been experimentally investigated was the one of a single spherical particle in front of a planar surface, as shown in Fig. 1.1. However, we remark that all these measurements were performed using TIRM[1, 12]. One of the drawbacks of such technique is that, it cannot be applied to the study of single particles in bulk or to the interaction between multiple particles. In this proposal we plan to use other techniques

such as photonic force microscopy[13] and digital video microscopy[14] (see below) to overcome just these limitations and gain further insights in phenomena involving critical fluctuations, in general, and critical Casimir forces, in particular. Therefore, in order to overcome the limitations of TIRM, we have adopted the use of multiple optical tweezers and digital video microscopy.

After having realized the experimental setup, as a first step, we have studied the critical Casimir forces arising between two particles in bulk. Then we proceeded to the investigation of the many-body forces arising between three particles arranged in a triangular configuration in bulk. We have performed these measurements using mesoscopic Brownian particles immersed in a critical mixture composed of water and 2,6-lutidine. In fact, this mixture is ideal as the characteristic length-scale ξ and time-scale τ of the critical fluctuations in a critical water-2,6-lutidine mixture (Fig. 1.1) are compatible with the measurable range of accessible by optical tweezers[15, 16, 17, 18, 19] and digital video microscopy[14].

Here, the theory for the study of many body interactions in critical Casimir forces will be discussed first (Chapter 2). Then, the established experimental setup will be described in detail (Chapter 3). Finally, the experimental measuerements that we have performed will be prenseted (Chapter 4).

Chapter 2

Theory

In order to detect the possible emergence of many-body critical Casimir forces, it is convenient to compare the experimental data with the predictions corresponding to pair-additivity: whatever (statistically signicant) is in excess to them is a genuine many-body effect. In a later step, one can try to compare with the available predictions for many-body effect which, however, at the present stage are not yet quantitatively reliable.

The basic strategy is to detect the forces looking at the statistics of the positions of two and then three colloids.

Two colloids: Let us indicate by $\vec{R}_i = (x_i, y_i, z_i)$ the position in the three-dimensional space of the $i-th$ colloid, of diameter d_i. For simplicity we shall assume below that $d_1 = d_2 = d$ i.e., that the two colloids are equal. The total potential felt by each of the two colloids results from

(a) single-particle forces:

  (1) *optical potential* V_{opt} and

  (2) *buoyancy* V_g;

(b) interactions:

(1) *electrostatic (and possibly van-der-Waals) interaction* V_{el} and

(2) *critical Casimir interaction* V_{Cas}.

While forces (a) are expected to be additive (in the case of V_{opt} the validity of this assumption depends on the distances among the particles involved), this is not the case for forces (b).

(a1) Optical potential: For a colloidal particle with center at a spatial point $\vec{R} = (x, y, z)$, this potential is well approximated by

$$V_{Opt}(\vec{R}; \vec{R_0}) = \frac{k_{xy}}{2}[(x - x_0)^2 + (y - y_0)^2] + \frac{k_z}{2}(z - z_0)^2 \tag{2.1}$$

where $\vec{R}_0 = (x_0, y_0, z_0)$ indicates the center of the optical trap, while k_{xy} and k_z are the spring constants of the trap on the xy-plane and along the z-direction, which are in principle not equal. Further below we estimate k_{xy} on the basis of the available data.

Note that at first sight one might be tempted to neglect the motion along z. However, when considering the interaction between two or more colloids, their vertical displacements might contribute significantly to the inter-particle (surface-to-surface and center-to-center) distance which controls the inter-particle interaction. Accordingly, one should have an hold on this. A vertical displacement $(\Delta z)_{op}$ of a particle trapped in V_{op} occurs as long as the corresponding potential is less, say, than $\simeq 2k_BT$ (being k_BT the natural scale of energy) and therefore one can estimate as $(\Delta z)_{op} \simeq 2(k_BT/k_z)^{1/2}$ the typical value of such a displacement. This, in turn, can be neglected only as long as it is much smaller than the distances relevant for setting the interactions.

(a2) Buoyancy: Due to gravity and the mismatch between the colloid and the solvent densities, a particle feels the potential

$$V_g = g_{eff} z + constant \tag{2.2}$$

where we assume z to be the vertical coordinate (and also the axis of anisotropy of

the optical trap, see above) and g_{eff} is an effective gravitational constant resulting from both radiation pressure and the density mismatch between the particle and the solvent density. In the experiments with TIRM reported in Ref. [5] one finds $g_{eff} \simeq 7k_BT/\mu$m and $\simeq 10k_BT/\mu$m for colloids of 2.4μm and 3.7μm of diameter. Due to the presence of the vertical trapping, the height z of the colloid fluctuates of a typical amount $(\Delta z)_{op}$ (see above). If the corresponding variation $g_{eff}(\Delta z)_{op}$ of V_g is negligible compared to the corresponding one of $\Delta V_{op} \simeq 2k_BT$ (see above), then one can neglect completely the effects of V_g. This would require to have $g_{eff} \ll (k_z k_B T)^{1/2}$.

(b1) Electrostatics: According to Ref. [20], the electrostatic interaction between two colloids at a surface-to-surface distance l takes the form (under the assumptions mentioned below)

$$V_{el}(l) = \frac{d^2 l_d^2}{\epsilon\epsilon_0} e^{-l/(l_d)} \tag{2.3}$$

where σ is the surface charge density of the colloid (e.g., $\sigma = 0:03C/m^2$ in the experiment of Ref. [21, 10] with diameter d = 0.4 m), l_d the Debye screening length, and ϵ the relative (static) dielectric constant of the mixture, which can be estimated as discussed further below and gives $\epsilon \cong 25$ for a critical water-lutidine mixture close to the critical point (we assume here that the dependence of ϵ on temperature can be neglected for the present purposes). We remind that $\epsilon_0 = 8,85 \times 10^{-12} C^2/(Jm)$. The Debye screening length is determined by (see Eq. (12.39) in Ref. [8])

$$l_D = \left(\frac{\epsilon\epsilon_0 k_B T}{2\rho_\infty e^2} \right)^{1/2} \tag{2.4}$$

in terms of the number density ρ_∞ of the 1:1 electrolyte which is present in the mixture and the elementary charge e. Given that no salt has been added to the mixture, ρ_∞ refers to the ions which result from the self-dissociation of the salt-free water-lutidine mixture, which has been estimated in Ref.[22] and it results in $l_D \cong 10nm$. The values found in the experiments reported in Ref[21] (indicated as κ^{-1} in Tab. II therein and obtained by fitting the measure potentials with

the exponential law predicted by Eq. (2.3), see also below) range from $10nm$ to $18nm$. In fact, for practical purposes, it is more convenient to parametrize the electrostatic interaction as

$$V_{el} = k_B T_C e^{-(l-l_l)/(l_d)} \tag{2.5}$$

where l_d and l_l are treated as fitting parameters. ($k_B T_C$ is introduced in this expression in order to set the energy scale.) Once they have been determined from the experimental data, one can compare their values with the ones that are expected on the basis of equation (2.3) and (2.4) above which, however, involve some parameters (such as, e.g., the colloid surface charge and the density of ions) which are diffcult to determine directly in experiments. This is the procedure that was followed,e.g., in Ref. [21] for fitting the electrostatic contribution (in conjunction also with a negligible van-der-Waals term) in the case of a colloid-substrate interaction (which, up to an overall factor 2, is the same as Eq. (2.3), at least within the Derjaguin approximation mentioned further below) and resulted in the parameters reported in Tab. II therein (with the change of notation $l \to z, l_{el} \to z_{es}$). In particular, it was found $l_{el} \cong 90$ or $l_{el} \cong 130nm$, depending on the involved colloid and therefore also in the present case one should expect similar values (reduced by $l_d ln2$), unless there are significant differences in the surface charges of the present colloids from those used in Ref.[21].

Approximations: The expressions (2.3) and (2.5) for the electrostatic interaction are valid under two major assumptions, i.e., *(i)* low surface (electric) potential $\Psi_0 \leq k_B T/e \cong 25mV$ at $T \cong 300K$ (such that the linearized Debye-Hückel theory applies) and *(ii)* the Derjaguin approximation $l << d/2$, which allows one to derive the interaction potential between two colloids (with diameter d) from the one between tho at surfaces. The validity of (i) can be checked a posteriori by taking into account that under this assumption $\Psi_0 = \rho l_D/(\epsilon\epsilon_0)$. For the polystyrene colloids used in Ref. [5], with $d = 2,4m$, the nominal surface charge was rather high: $\rho = 10C/cm^2$, which therefore gives $\Psi_0 \cong 5V$ for $l_D = 10nm$ and $\epsilon \cong 25$. Accordingly, the previous approximation did not work for that case. Even if (i) is not fulfillled, the form of the interaction potential is still given by

Eq. (2.3) as long as $l > l_D$ but with an effective surface charge $\rho^* = \rho_s^* g(\rho/\rho_s)$ with $g(x) = 2x/[1 + \sqrt{((2x)^2 + 1)}]$, which depends on $x = \rho/\rho_s^*$ and for $>> \rho_s^*$ saturates the value $\rho_s^* = 4\epsilon\epsilon_0 k_B T/(el_D) \cong 0.24 C/cm^2$ for the present mizxture with $l_D \cong 10nm$ for a colloid with $d = 2m$, which is in qualitative agreement with the figures found in Ref. [5]. Due to the possible emergence of this complication with the surface charge, it is indeed convenient to proceed with a fitting of the electrostatic with the form in Eq. (2.5) and then verify a posteriori if the corresponding figures are within an acceptable range of values.

Dielectric constant: The dielectric constant ϵ of the water-lutidine mixture enters into Eqs. (2.3) and (2.4). In the absence of a direct determination, it can be calculated by knowing that the lutidine volume fraction, ϕ_L in the critical mixture is, $\phi_L \cong 0.25$ (see, e.g., Ref.[5, 1]), that the dielectric constants of pure water and pure lutidine are, $\epsilon_W = 81$ and $\epsilon_L = 7.33$, respectively (see, e.g., Ref. [23]). By using the Clausis-Mossotti formula for mixing and by neglecting the fractional volume change on mixing, one finds that $f(\epsilon) = \phi_L f(\epsilon_L) + (1 - \epsilon_L) f(\epsilon_W)$ where $f(x) = (x - 1)/(x + 2)$, which yields $\epsilon \cong 25.5$.

Chapter 3

Experimental Setup

Light can exert a force on matter due to momentum exhange via scattering[24]. And after the invention of laser, Arthur Ashkin prosed a technique "single-beam gradient force trap" as he called, to make use of radiation pressure[25] and optical gradient forces[26] in 1970. Now, optical tweezers has many applications in variety of areas from biophysics[27, 28, 29, 30] to optical lattices[31, 32], sensing applications[15, 16, 17, 33, 34] to atomic trapping[16, 35, 36].

Here we employed optical tweezers in order to measure the nanoscalled critical Casimir forces. Our experimental setup consists of three main parts: Trapping optics, imaging optics and temperature controlling unit (See Fig. 3.2). Trapping optics part includes holographic optical tweezers setup, and the second part of the setup is a home-built light microscope, which is used to track particles by employing digital video microscopy technique (see the next Chapter). Final part of the setup is the temperature control unit that allows us to control the temperature of sample with a precision of $2mK$ (at room temperature) by using a Proportional Integral Derivative (PID) feedback controller.

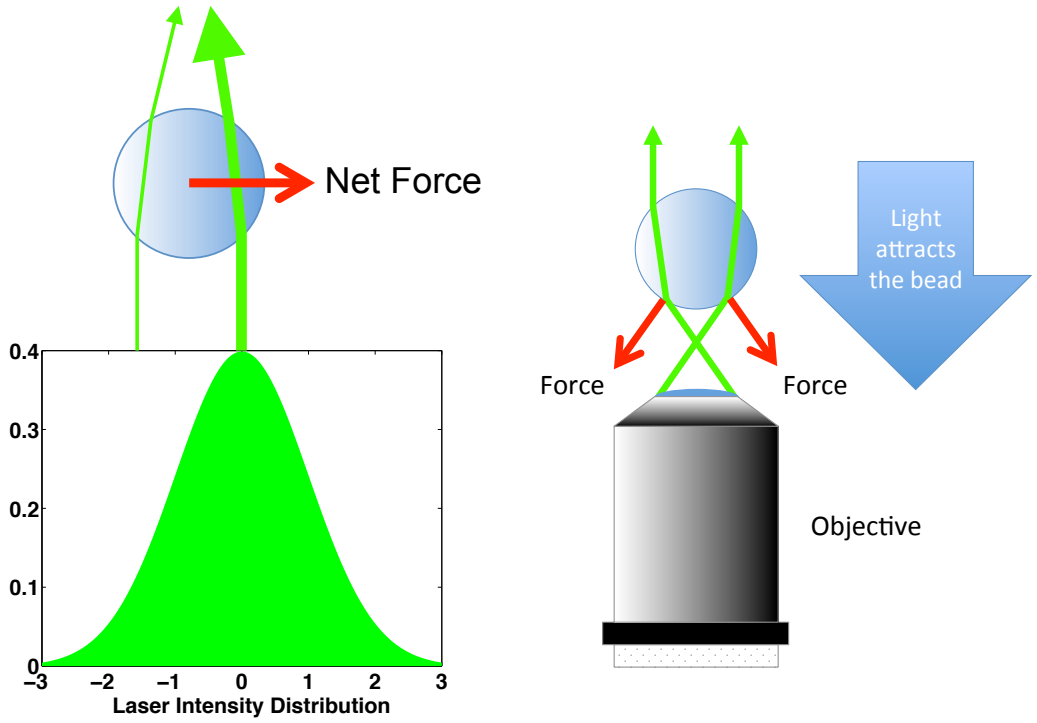

(a) (b)

Figure 3.1: Gradient(a) and scattering(b) forces. *(a) Light is scattered from particle due to refractive index mismatch and more momentum is transfered from higher intensity. Therefore, particle is attracted to the higher intensity. (b) Highly focused laser light creates an axial gradient additional to Gaussian beam profile of laser and attracts the particle towards focal point because of momentum conservation.*

3.1 Holographic Optical Tweezers

The focusing of the resulting beam is achieved by using a high-numerical aperture (NA=1.30) oil-immersion objective, as shown in the schematic presentation in Fig. 3.2. Holographic optical tweezers differ from conventional optical tweezers because they allow to create dynamic and multiple optical traps at the same time by multiplexing a single laser beam. This beam shaping can be managed by using a Spatial Lightt Modulator (SLM). The resulting optical traps can be well controlled both in time and space.

SLM shapes the incoming beam adding an additional phase to it. This is

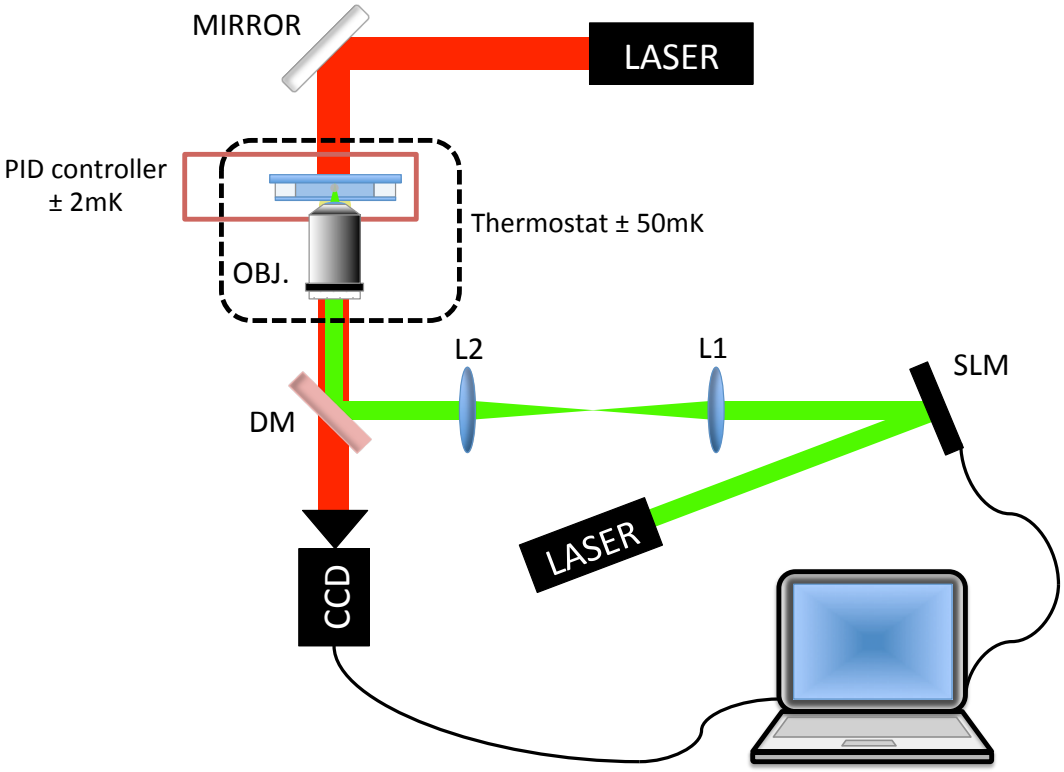

Figure 3.2: Schematic representation of holographic optical tweezers setup. *First order reflected beam is selected via 1:1 telescope with lenses (L1 and L2) and coupled inside the objective with the help of dichroic mirror(DM). Objective and sample is inside thermally controlled environment and fine tuning of the temperature is done by PID controller.*

done by the active part of the SLM, which is essentially a pixilated screen, where each pixel can alter the phase of the light impinging on it. This screen can be controlled by a computer, essentially like a standard video projector. An SLM works either in reflection or in transmission mode. SLMs that work as transmissive are commonly used in overhead projectors and are cheaper, but achieve relatively low light deflection efficiency. SLMs that work in reflection tends to achieve much higher modulation efficiency (up to about 85%). SLMs are classified as Electrically Addressed Spatial Light Modulator (EASLM) or Optically Addressed Spatial Light Modulator (OASLM). OASLMs use liquid crystals to

replicate the optical beam shined on the surface, while EASLMs are electronically controlled and uses the conventional inputs from computers like VGA input. All kinds of SLMs have been widely used for applications going from beam shaping (e.g. measurement of ultrafast pulses, creating tractor vector beam) to optical data storage[37, 38, 39].

For this work, as in most optical trapping applications[40, 16, 37], we decided to use an EASLM that works in reflection mode in order to achieve high deflection efficiency and being able to control it using a computer interface. In particular, we used an EASLM produced by HoloeyeGmbH (HoloeyePLUTO-VIS) to modulate the phase of the laser light. The SLM is controlled by a home-made computer program to create multiple optical traps.

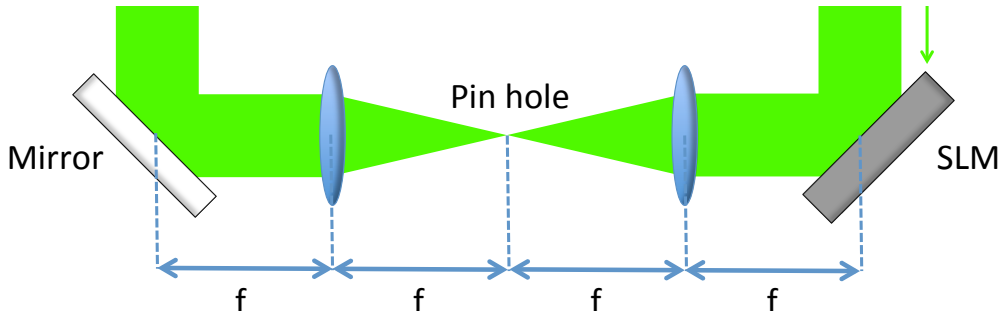

Figure 3.3: SLM working principle and 4f configuration. *The phase image projected on the SLM screen is the Fourier transform of the intensity distribution in the focal plane. For example, a set of three optical traps can be generated with the grating phase mask shown in Fig. 3.4 (c). The laser beam is transferred to the objective back-focal plane by a 1:1 telescope constituted by two lenses.*

There are several ways to generate multiple traps. The basic idea is to project an image on the SLM, which is the Fourier transform of the light distribution required in the objective focal plane. The basic scheme for such configurations is shown in Fig. 3.3. In this way, by taking the Fourier transform of the image via lens, multiple parallel propagating beams can be created on the first order refracted beam so as the multiple highly focused laser beam on the focal point of the objective which led us to have the control of all optical traps. There are several possible algorithms to generate these phase images[41]. In particular, we have investigated two of these algorithms: the plane-wave superposition (PWS) algorithm and the Gerchberg-Saxton (GS) algorithm.

Some examples of holographic phase masks generated with Gerchberg-Saxton (GS) technique are shown in Fig. 3.4.

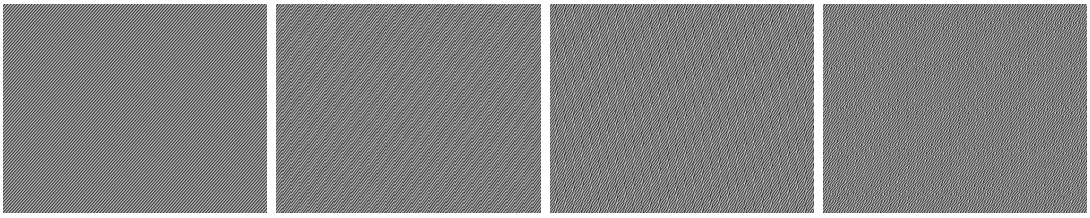

(a) **(b)** **(c)** **(d)**

Figure 3.4: Examples of phasemasks. *The holograms were created with Gerchberg-Saxton (GS) algorithm in Matlab. SLM creates a single focal point with hologram (a), two focal points with (b), triple focal point with (c) and 4 focal points with (d).*

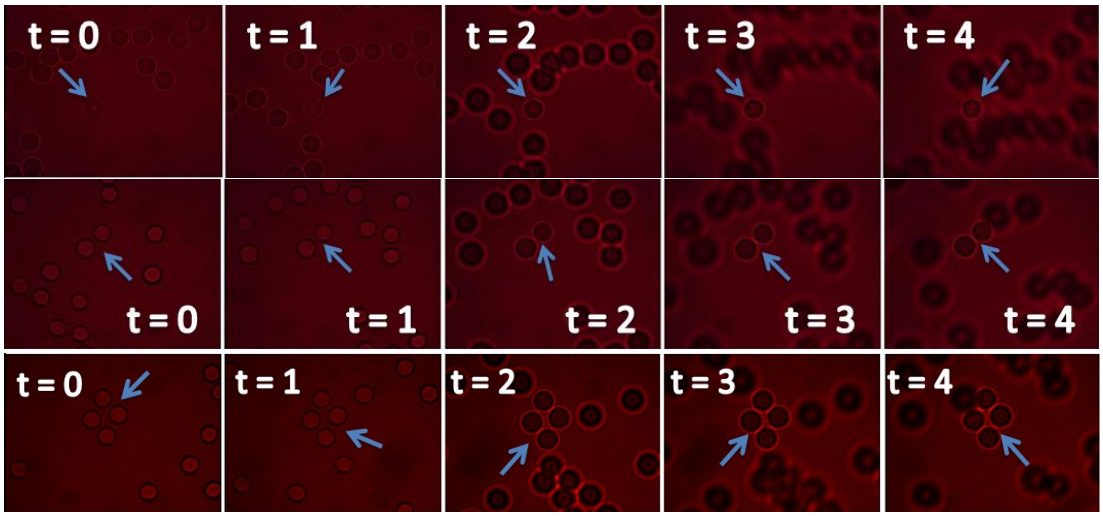

Figure 3.5: Real time snapshots for multiple partical trapping. *One, two ($d = 2.1\mu m$) and three particles ($d = 5\mu m$) are trapped at the same time and moved in 3D.*

3.2 Imaging Optics

Optimized home-made microscope was built and high-numerical aperture ($NA = 1.30$) oil-immersion objective with $100x$ magnification was used for both trapping purposes by focusing the shaped laser beam and imaging the sample using a digital camera. For the illumination, we used He-Ne laser source (wavelength $633nm$).

In fact, the use of a coherent illumination simplifies the tracking procedure by digital video microscopy, since coherent light is very sensitive to the change in spatial position of the particles due to scattering. Laser light was collimated and directed on the sample using a series of lenses and mirrors and the transmitted light collected by the objective and was separated from the trapping laser light via dichroic mirror. Then the trasnmitted light was projected on a CCD camera for further digital processing of the images with Matlab. By taking the advantage of this configuration, we are able to track colloidal particles with radius between 1 and $5\mu m$ within $15nm$ precision.

3.2.1 Digital Video Microscopy

The videos acquired with our digital video microscopy setup and are analyzed by home-made software which is programmed in Matlab. The software includes three packages:

(A) *Frame by frame particle identification*

(B) *Tracing*

(C) *Trajectory extraction*

3.2.1.1 Frame by frame particle identification

This package identifies the particles present in each frame, one frame at a time. The algorithm main steps are the following:

1) Extraction of the video background.

2) Subtraction of the background from each frame.

3) Transformation of the color image into a black-and-white image.

4) Identification of the particles (This is based on the brightness differences between the background and the particles in the video. The sensitivity to the particle size can be adjusted through the codes in order to reject false signals).

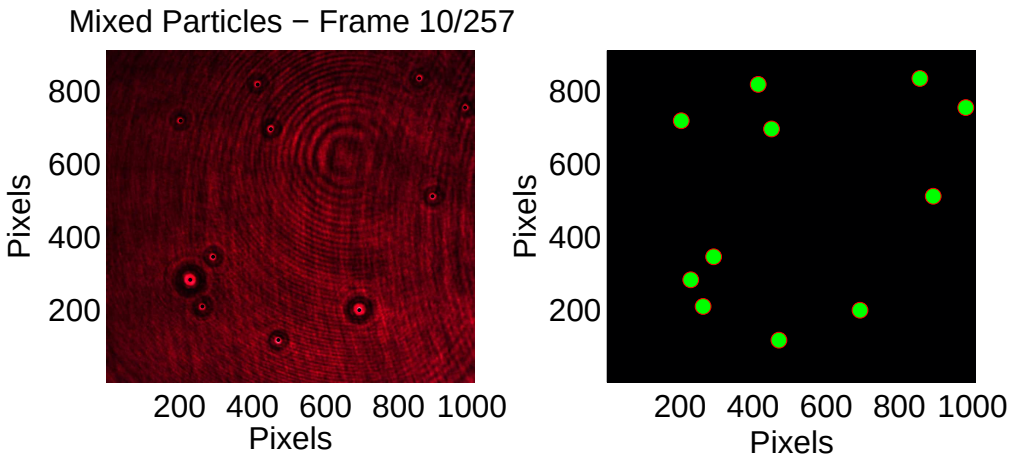

Figure 3.6: Digital video microscopy. Particle tracking at work. *The images on the left are acquired videos and the images on the right are the analized images with the particles positions identified. Note the presence of three different particles of different sizes.*

3.2.1.2 Tracing

Tracing package identifies sequences of particle positions that correspond to the same particle across frames (See Fig. 3.7 (a).)

3.2.1.3 Trajectory Extraction

Finally, the traces are combined to reconstruct the trajectories of the various particles which have physical units both for the position and the time (See Fig. 3.7 (b)).

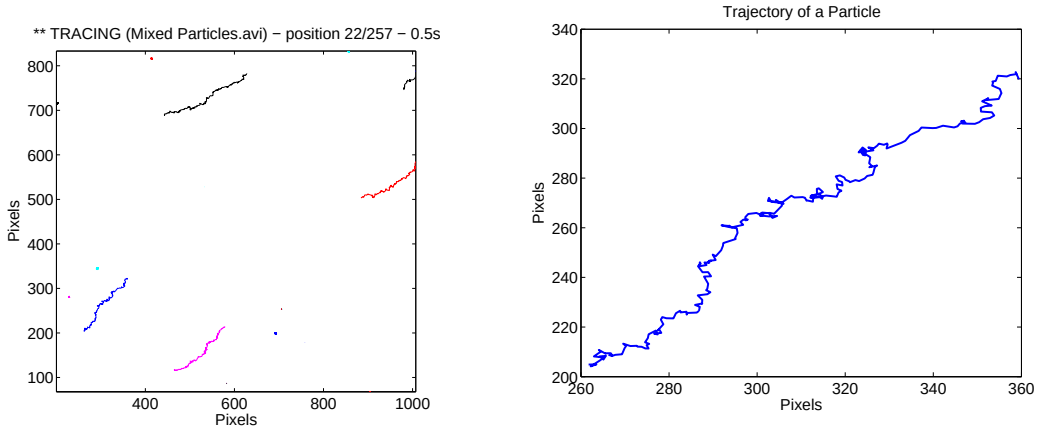

(a) **(b)**

Figure 3.7: Digital video microscopy. Particle tracing(a) and particle trajectory(b). ***(a)****Screenshot of the tracing software package at work. The positions of the particles in successive frames are connected in order to reconstruct traces.****(b)****Screenshot of a trajectory reconstructed by our software.*

3.3 Temperature Controlling Unit

Critical Casimir forces caused by the confinement of critical fluctuations can be measured in a critical mixture of water and 2,6-lutine[1] and such critical fluctuations are very sensitive to small temperature changes. Therefore, one needs to achieve very fine control of the temperature in order to perform such kind of experiments (within a few miliKelvin at room temperature) which makes this one of the most challanging parts of the experiment. In order to have the stability within 2 to $5mK$, we need a thermally isolated environment as well as a high-precision feedback temperature controller. Hence, we have enclosed our system with a thermally stabilized box in order to avoid any air flow which may produce instability on the sample temperature and we have also isolated the sample holder from the xy-stage to avoid from the thermal contact. At the same time, since we are heating/cooling the sample through the objective, we made a good thermal contact between objective and thermoelectric cooler (TEC Element), which our temperature controller uses as heating/cooling element, inside an isolated enclosed system (See Fig. 3.2).

Temperature controlling system includes two parts: Thermostat and PID controller. Thermostat keeps the sample holders' temperature stable within $50mK$ by flowing water through water channel inside home-made copper sample holder. In order to increase the temperature stability of the system down to $2mK$, we used Proportional Integral Derivative (PID) controller produced by Thorlabs (Model: TED 4015). PID controllers use feedback loop to keep the temperature at the desired value by calculating the error between set value and measured value of temperature and responding accordingly. PID controllers response is the combination of 3 different responses to an error[42, 43]. The first one is a proportional response. Here, response to an error is proportional with some constant in front called proportional gain (tuning parameter):

$$P_out = K_p e(t), \tag{3.1}$$

where K_p is proportional gain and $e(t)$ is the error, namely

$$e(t) = SetPoint(SP) - ProcessVarible(PV) \tag{3.2}$$

Therefore, if the error was large, the resulting response was accordingly large. However, the drawback here is that; when the error is too large, it may cause instability of the system, and also, if the error is too small, the response may not be sufficient to effectively control the system temperature. Proportional only controller's behaviour can be seen in Fig. 3.8.

The second term in the PID controller is so called integral term and is proportional to the integral of the error. Thus, the integral response of a PID controller sums the error over sometime:

$$I_out = K_i \int_0^t (e(\tau))d\tau, \tag{3.3}$$

where K_i is integral gain and $e(\tau)$ is the error integrated between time 0 and t. Here, since the cumulative error is calculated, it faster to reach steady state

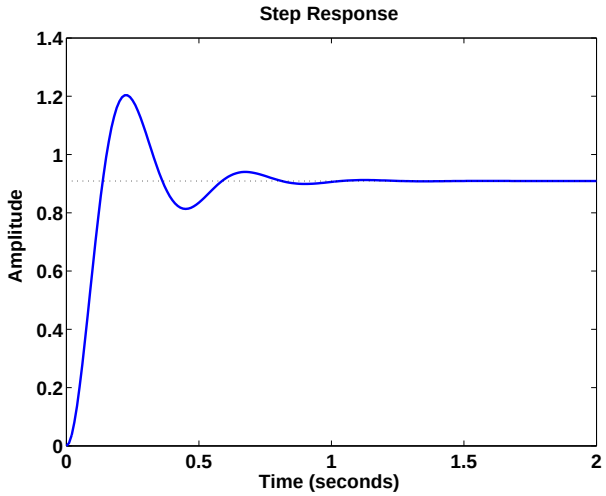

Figure 3.8: Proportional controller response. *Pure proportional controllers amplitude of response with* $K_p = 200$ *and* 0.01 *second time resolution.*

and eliminates steady state error which is unlikely in proportional controllers. However, due to the summation of error over time and lack of derivative term, there is a trade off between less overshooting and settling time (See Fig. 3.9).

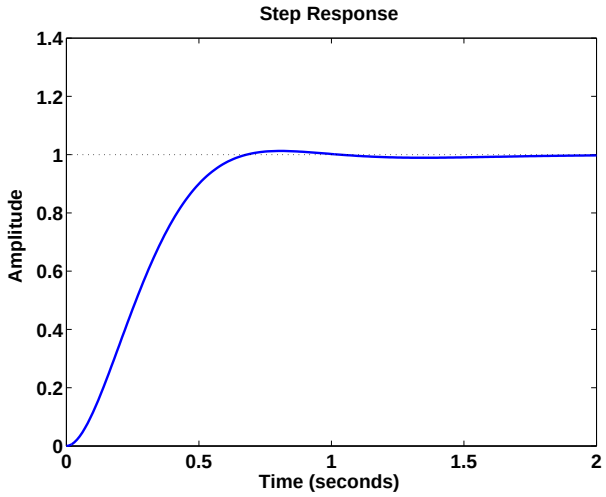

Figure 3.9: Proportional integral controller response. *Proportional Integral controllers response with* $K_p = 30$, $K_i = 70$ *and* 0.01 *seconds time resolution.*

The third, derivative term of the PID controller responses proportional to derivative of the error in time:

$$D_{out} = K_d \frac{d}{dt} e(\tau), \tag{3.4}$$

where K_d is the derivative gain and $e(t)$ is the error in time. This term permits one to improve the response time of the system.

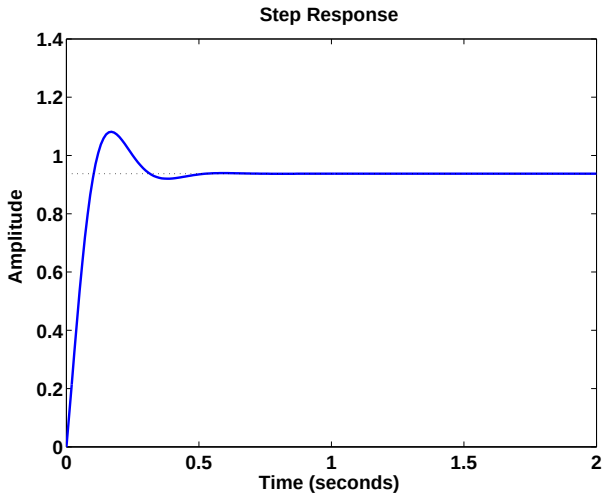

Figure 3.10: Proportional derivative controller response. *Response of Proportional Derivative controller with* $K_p = 200$, $K_d = 5$ *and* 0.01 *seconds time resolution.*

Therefore the overall response of the PID controller is the summation of these three terms which can be expressed as

$$u(t) = K_p e(\tau) + K_i \int_0^t (e(\tau))d\tau + K_d \frac{d}{dt} e(\tau) \tag{3.5}$$

The optimum behavior of the PID controller can be adjusted by changing the tunable parameters in the equation as well as setting the delay time of the controller depending on both purpose of use and the system employed. Overall response with optimized parameters for our experiments is shown in Figure 3.11 (Step reponses were calculated according to Ref.[42] with real parameters used in our experiments).

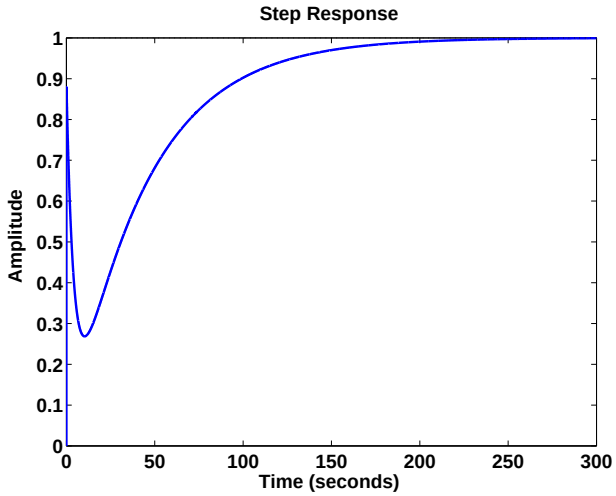

Figure 3.11: PID response. *Response of PID controller with* $K_p = 3.297$, $K_i = 0.50$, $K_d = 80$ *and* 0.01 *seconds time resolution.*

There are several ways to tune PID controllers and Ziegler−Nichols method[44] introduced in the 1940s is the most famous one. Here, integral (K_i) and derivative (K_d) terms set to zero and proportional gain (K_p) increased until it reaches the ultimate gain where the output of the system oscillates with constant amplitude[45]. Then, K_i and K_d terms are adjusted accordingly depending on the controller type and the applied system.

PID Response Table					
Parameter	**Rise time**	**Overshoot**	**Settling time**	**Steady-state error**	**Stability**
K_p	Decrease	Increase	Increase	Decrease	Degrade
K_i	Decrease	Increase	Increase	Eliminate	Degrade
K_d	Decrease	Decrease	Decrease	No effect	Improve

Table 3.1: PID response table. *The effect of the parameter increments.*

Chapter 4

Experimental Measurements

In this Chapter, experimental results concerning the interactions between spherical colloids with various dimensions in a critical mixture are presented and holographic optical tweezers are used as force measurement tool.

4.1 Brownian Motion & Calibration of an Optical Trap

Particles in fluid moves with different velocities in different directions due to the collusions between particle and fluid molecules. This random motion is called Brownian motion and has zero mean of the force acting on particle because of the uncorrelated collusions with surrounding molecules[46].

The colloidal particles used in our experiments are passive mesoscopic Brownian particles immersed in a critical mixture of water-2,6-lutidine. Therefore, these particles are subject to following Langevin equation:

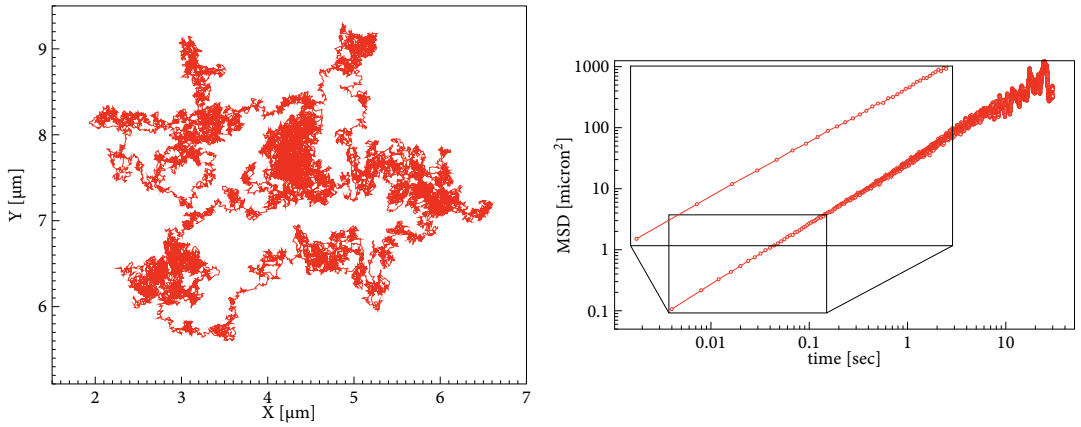

Figure 4.1: Trajectory of a free diffusive Brownian particle and MSD grapgh. *Trajectory of a Brownian particle in water-2,6lutine solution (a), and the corresponding Mean Square Displacement(MSD) grapgh (b).*

$$m\frac{d^2x}{dt^2} = -\lambda\frac{dx}{dt} + \eta(t) \tag{4.1}$$

where m is the mass of the particle, x is its position, λ is its viscosity and η is the noise term which represents the collisions between the liquid molecules and the particle. The noise term has Gaussian probability distribution with correlation function

$$\langle \eta_i(t)\eta_j(t')\rangle = 2\lambda k_B T\delta_{i,j}\delta(t-t') \tag{4.2}$$

where k_B is the Boltzmann constant and T is the absolute temperature. Einsteins relation holds, i.e.,

$$D = \mu k_B T \tag{4.3}$$

where D is the particle diffusion constant and μ is the particle mobility. This is known as fluctuation-dissipation theorem[47] and can be reduced into the Stokes-Einstein relation to be used in small Reynolds number as

$$D = \frac{k_B T}{6\pi\eta r} \tag{4.4}$$

where r is the radius of the particle. Therefore, a freely diffusing particle is subject to Stokes-Einstein relation and has a linear Mean Square Displacement (MSD) which is commonly used as characterization tool for random motions.

A particle in an optical trap would feel external restoring force depending on the optical potential. So the equation of motion for a Brownian particle in an optical trap becomes

$$m\frac{d^2x}{dt^2} = -\lambda\frac{dx}{dt} + \eta(t) - kx \tag{4.5}$$

where k is the stiffness of the trap. Therefore, a Brownian particle has a Gaussian probability distribution in two dimensions and has an eliptical distribution in the $z - direction$ because of the less trap stiffness in lateral direction compare to the axial directions[48].

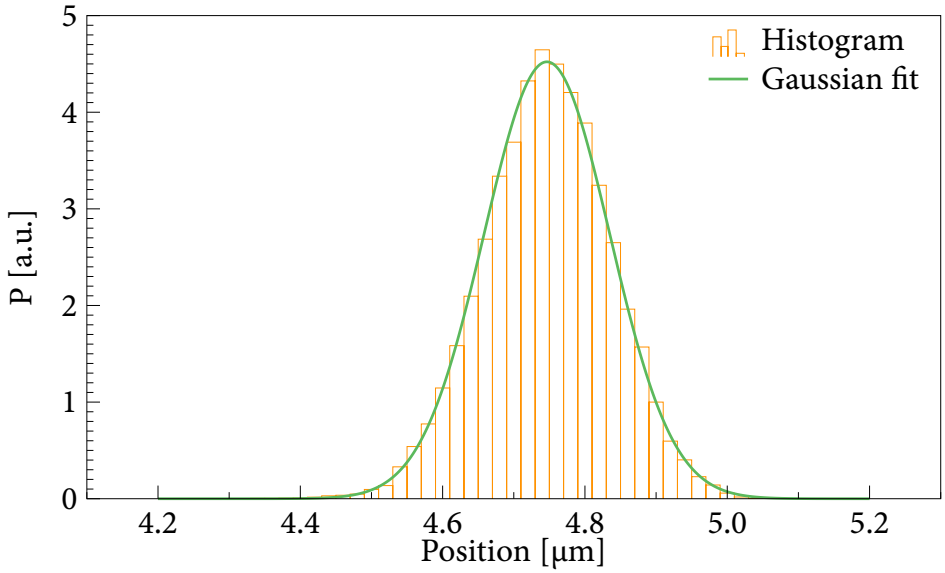

Figure 4.2: A Brownian particle in an optical trap. *Probability distribution of a Brownian particle around trap center follows a two dimensional Gaussian distrbution*

The stiffness k of an optical trap is linearly depended on the optical power of trapping beam and also defines the characteristics of the optical tweezers. There are several ways to calibrate an optical trap[49, 50, 51, 52].

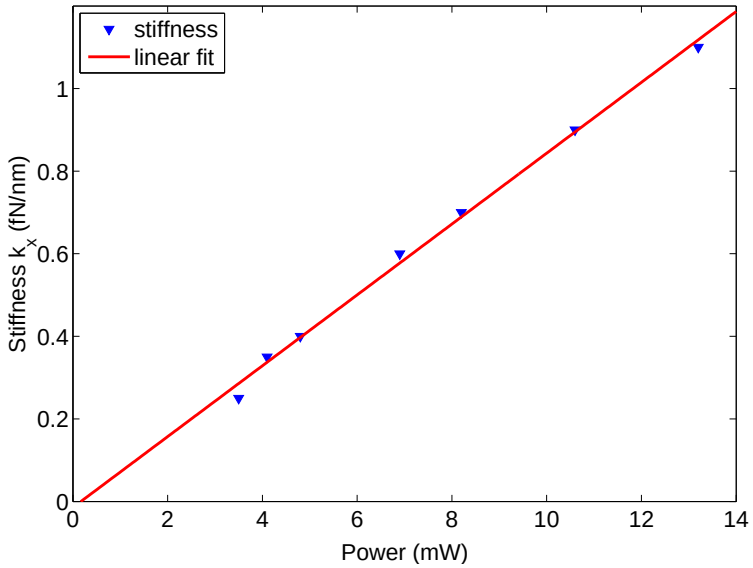

Figure 4.3: Optical trap stiffnes as a function of laser power. *Stiffness of an optical trap is linearly depended on the optical power put on the trap.*

4.1.1 Calibration of an Optical Trap with Equipartition Method

The equipartition theorem relates the temperature of the system with the average energy if the system is in thermal equilibrium. This theorem states that the energy of a Brownian particle at thermal equilibrium with a heat bath can be estimated as the average total energy used as in the case of molecules of an ideal gas. Since our optically trapped particle is in thermal equilibrium with its surrounding medium, which is very large compare to particle, the stiffness of the optical trap can be estimated by equating the energy of the system to energy of an optical trap. If the trap is assumed to be harmonic, one gets

$$\langle U(x)\rangle = \frac{1}{2}k_x\langle(x-x_0)^2\rangle = \frac{1}{2}k_BT. \tag{4.6}$$

Thus, if the statistical variance in the x-direction $\langle(x-x_0)^2\rangle$ and the temperature T of the system are known, trap stiffness k_x can be estimated as

$$k_x = \frac{k_B T}{\langle (x - x_0)^2 \rangle} \tag{4.7}$$

4.1.2 Calibration of an Optical Trap with Potential Analysis Method

A Brownian particle in an optical trap has a Gaussian distribution in x and y directions. Therefore, the data acquired by Digital Video Microscopy technique should have a Gaussian probability distribution. It is possible to deduce the shape of the potential through histogram of optically trapped particle in thermal equilibrium. The probability density function is described by Boltzmann distribution as

$$\rho(x) = \frac{e^{-\frac{U(x)}{k_B T}}}{Z} \tag{4.8}$$

where k_B is Boltzmann constant, T is absolute temperature and Z is a normalization constant.

Since the probability distribution is obtained by experiment, potential can be found as

$$U(x) = -k_B T ln(Z(x)) \tag{4.9}$$

and the potential, if harmonic, is related to stiffness with the equation

$$\langle U(x) \rangle = \frac{1}{2} k_x \langle (x - x_0)^2 \rangle \tag{4.10}$$

Hence k_x can be found as

$$k_x = -\frac{2 k_B T ln(Z\rho(x))\pi r^2)}{\langle (x - x_0)^2 \rangle} \tag{4.11}$$

4.1.3 Calibration of an Optical Trap with Correlation Method

According to Wiener-Kintchine theorem, power spectral density is related to autocorrelation function by

$$r_{xx}(\tau) = \langle x(t+\tau)x^*(t)\rangle = \frac{k_B T}{x} e^{-\frac{k_x}{\lambda}|\tau|} \tag{4.12}$$

where λ is the viscosity denoted in the Langevin equation. Therefore, by fitting the experimental autocorrelation function to the theoretical value given with above equation, trap stiffness can be estimated.

4.2 Preliminery Procedures

4.2.1 Sample Preperation

Critical mixture can be prepared by mixing the specific constituents certain portion. Here, we have used water and 2,6-lutidine critical mixture which is widely used and has well known spesifications[1, 5, 21, 53]. According to coexisting phase diagram given in Ref.[1] for water-2,6 lutidine, lower critical point is about $c_L = 0.286$ and therefore, lutidine was added with a mass fraction of 28.6 % over water filled glass tube.

Critical Casimir force measurements were done in a special glass micro channels with about $10\mu m$ height and $3cm$ long dimensions having two chimney type entrances. After the critical mixture is prepared, desired micro particles were added to the solution. After sufficient waiting time (at least 3 hours) the solution injected into the chamber and chimneys of the chamber were sealed with parafilm in a way that solution cannot evaporate. Parafilm were chosen as a sealing material because lutidine cannot solve it unlike most of the glues and plastic. Hence, sample can be preserved inside a micro-channel for a long time (at least 15 days

with good sealing) which gives us the opportunity of making the same condition experiments for days by using the exact same particles.

4.2.2 Experimental Procedure

Before starting the measurements, we first checked if the optical traps are stable enough both over time and increasing temperature. So, the preliminary experiments were started with a single particle in an optical trap and repeated for all other optical traps. After several measurements, it's been concluded that the optical traps' stiffness stay within 0.8% over time and 1% standart deviation range over temperature. Stability analysis were done both for single traps and relative distance between traps, yet results remain within 1% deviation.

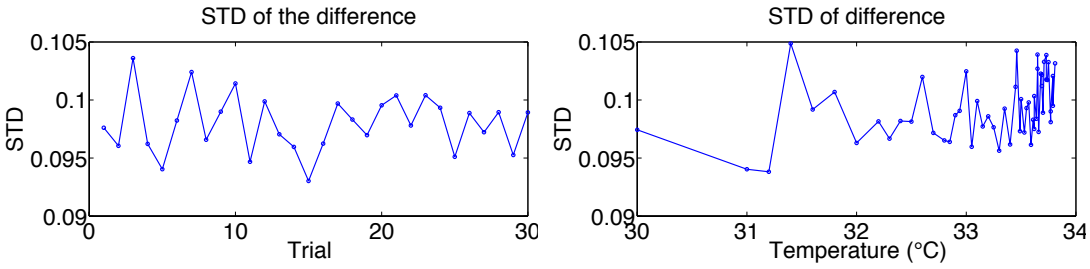

Figure 4.4: Optical trap stability analysis. *Standart deviation in the difference of trajectories were analysed for the stability control of the optical traps for both as a function of trial with each trial is 3 minutes(a) and temperature(b).*

To measure the critical Casimir forces, one needs to confine critical fluctuations when the separation between confining surfaces will become comparable with the correlation length. In order to get that condition, we have fixed the surface-to-surface distance l between colloids and increase the temperature gradually, namely increased the correlation length, so that we finally reach the point where the correlation length and the separation distance l are comparable[54, 55, 56].

First, we calibrated the optical traps in a way that we store the information about the original position of the traps without any kind of interaction. Then,

electrostatic interactions were measured which will be described in the next section so that one should become able to measure critical Casimir interactions. For the measurement of critical Casimir forces; first, we have trapped 2 particles with created optical traps and move about $3\mu m$ above the surface in order to avoid the effect of the surface. So, it is sure that the interaction is only between trapped particles, and then video recording process were started in order to analyse by digital video microcopy technique[14, 57] discussed in chapter 2.

Measurements were started at the nominal temperature of 30 °C (as read on the temperature controller) and continued until the particles got stuck together which happes at about 33.18 °C which is just below the critical point. Measurements were done with gradually increasing temperature and the increment steps became smaller as it is getting close to the end point in order to be more precise. The videos were acquired for 3 minutes each and resting time between temperature increments for temperature stabilization was set to 6 minutes. Therefore, at the end of one set of measurements, we had a set of videos for different temperatures which allowed us to compare the case of detectable critical Casimir interactions with noninteraction regime.

4.3 Measurement of the Electrostatic Interaction

The electrostatic interaction between colloids seperated with a surface-to-surface distance l is predicted to be in the form[20]

$$V_{el}(l) = \frac{\pi d \sigma^2 l_d^2}{\epsilon \epsilon_0} e^{-\frac{l}{l_d}} \tag{4.13}$$

where σ is the surface charge density of colloid (e.g. $\sigma = 0.03 C/m^2$)[11] and l_d is the Debye screening length which was estimated to be $10nm$[5, 22]. Also ϵ is the relative dielectric constant and $\epsilon_0 = 8,85 \times 10^{-12} C^2/jm$. The Debye screening length is given by the formula[20]

$$l_D = \left(\frac{\epsilon \epsilon_0 k_B T}{2 \rho_\infty e^2} \right)^{1/2} \tag{4.14}$$

where ρ_∞ refers to the ions which result from the self-dissociation of the salt-free water-utidine mixture. Therefore, the electrostatic potential between colloidal particles can be written in form of

$$V_{el} = k_B T_C e^{-(l-l_l)/l_d} \tag{4.15}$$

as it is described in detail in Chapter 2.

In the calibration of the electrostatic force between two colloids, l_l and l_d are treated as fitting parameters in simulations to experimental results. The resulting values obtained after calibration are $l_d = 16nm$ and $l_l = 113nm$. In fact these values are in good agreement with the values found in the literature[21, 5], which can also be predicted from first principles[22].

Once the optical traps were calibrated (see the calibration subsection in this Chapter), we could perform the measurement of the electrostatic interaction between the two colloids. To perform the experiment, two nearby traps were created using the SLM and one trap left empty for the calibration process of the other trap with single particle. Once the measurements are done with one particle, the corresponding trap was emptied and the second particle was trapped within uncalibrated trap. Then, the calibration of the second trap was done and so information of both individual traps was stored. Then, both traps were filled with the same particles used in calibration processes and the same measurements were repeated. Therefore, the effect of particles to each other was investigated by checking the particles probability distribution inside the optical potentials. Here, the deviation from the original position (determined by the calibration measurement) tells about the the particles were effected from presence of other particle, in this case the effect is electrostatic repulsion. Also, the interaction between particles was investigated as a function of surface-to-surface distance in order to check the fitting parameters used in the theoretical calculations[58, 59, 60].

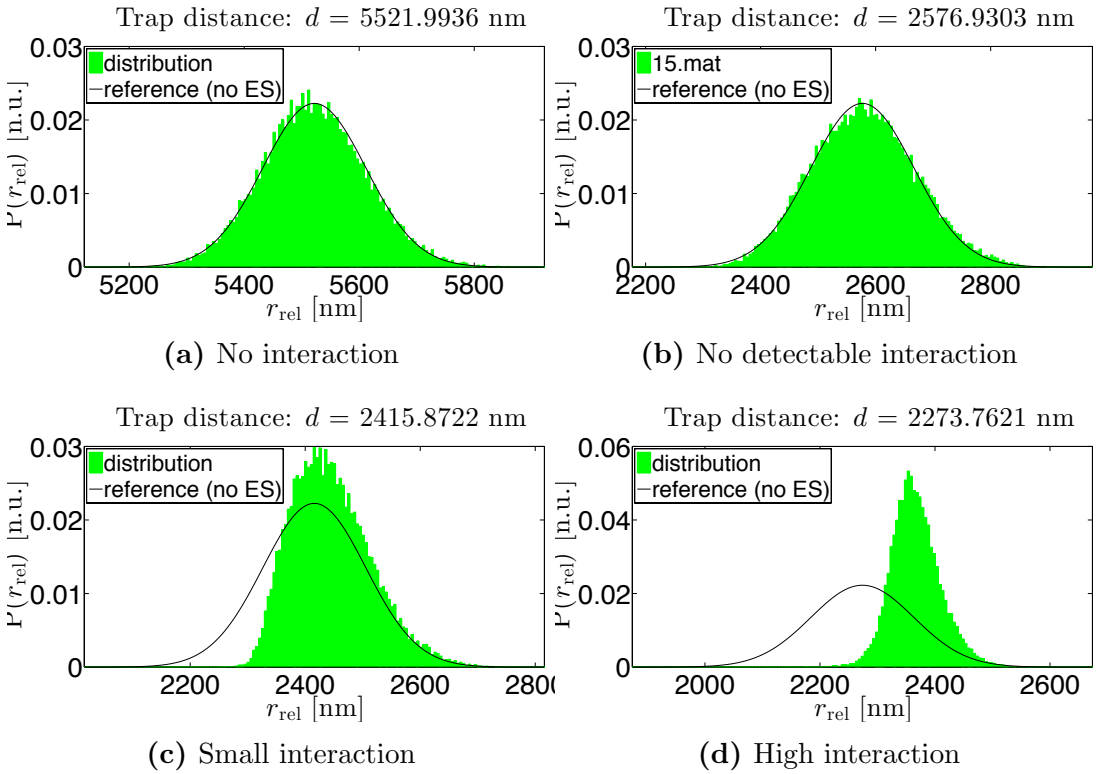

(a) No interaction **(b)** No detectable interaction

(c) Small interaction **(d)** High interaction

Figure 4.5: Electrostatic interaction of two colloids. *When the colloidal particles are apart ($\simeq 3.4\mu m$) there is no detectable interaction in between(a). However, when the particles get closer particles start to feel electrostatic interaction (c) and when they are close enough ($\simeq 200nm$) there is an asymmetric squeezing in histograms towards one side due to electrostatic repulsion between likely charged particles.*

For the analysis of the experimental data, the difference of trajectories was investigated in order to eliminate the common drift that may occur on both traps as well as the motion due to pointing instability of trapping laser. So, non-symmetric Gaussian distribution was expected from the histogram of the difference of trajectories due to electrostatic repulsion between like particles. Also, the electrostatic interactions were become irresolvable roughly after $250nm$ seperation between particles due to fast decay for electrostatic forces depending on distace.

As it is seen in the histograms, Gaussian distribution is squeezed on one side due to the electrostatic interaction between particles. Here, since the particles

are interacting through the surfaces facing each other, left side of the normalized probability distributions are squeezed towards the outside, namely particles are feeling a repulsive net force which allow us to determine the electrostatic parameters of the system so that we were able to measure pure critical Casimir interactions by subtracting the electrostatic interactions.

4.4 Measurement of Critical Casimir Forces

4.4.1 Background

In the presence of a critical mixture confined between two surfaces, attractive or repulsive forces can arise (depending on the boundary conditions, i.e., whether the surfaces are hydrophilic or hydrophobic). These are the so-called critical Casimir forces[5, 7, 61, 62].

In critical mixtures, as the temperature getting closer to the critical point, correlation length getting larger and finally diverges at the critical point. Correlation length is given by[5]

$$\xi(T) = \xi_0 \mid \frac{T - T_C}{T_C} \mid^{-\nu} \tag{4.16}$$

where $\nu = 0.63$ determined experimentally and $\xi_0 = 2.3 \pm (0.4\mathring{A})$ [1].

For the critical Casimir potentials V_{Cas} it is well known that within the Derjaguin approximation $l << d/2$ its expression for two identical spheres (at a surface-to- surface distance l) is half of the expression for a sphere in front of a plane, i.e.,

$$V_c(l) = k_B T \frac{d}{4l} \theta(l/\xi) \tag{4.17}$$

where $\theta(x)$ is the scaling function and can be read from Fig. 2 in Ref[5] as

$$\Theta(x) = \begin{cases} -9.425 x e^{-x} & for\ x \geq 6 \\ Q_6(x) + x(0.628319 - 1.74764x) lnx & for\ x < 6 \end{cases} \tag{4.18}$$

with

$$\begin{aligned} Q_6(x) = -2.57611 - 3.29886\,x + 2.27325\,x^2 + 0.2005\,x^3 \\ +0.010743\,x^4 - 0.0018317\,x^5 + 0.000072396\,x^6. \end{aligned} \tag{4.19}$$

within the first analytical approximation.

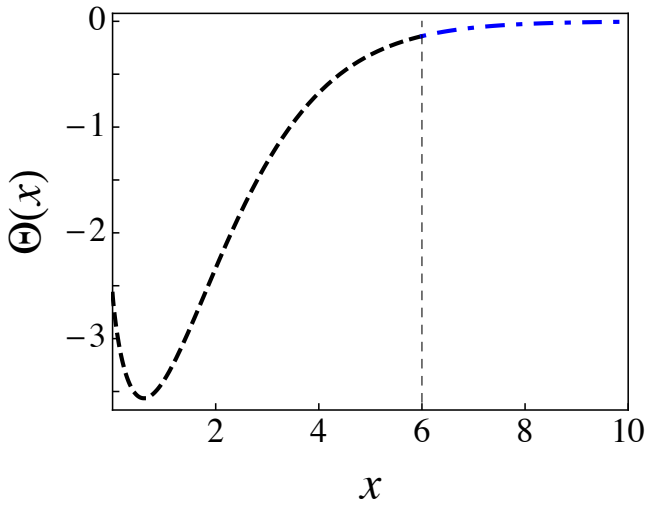

Figure 4.6: Scaling function $\Theta(x)$ of the critical Casimir potential for a sphere in front of a plate within the Derjaguin approximation. *This function can be derived $\vartheta_{\|}(x)(x)$ given in Ref.[4, 5, 2]. The dashed and dash-dotted lines correspond to the approximations provided by the analytic expressions in Eqs. (4.18) and (4.19) for $x < 6$ and $x > 6$, respectively*

4.4.2 Results

A Brownian particle in an optical trap has a Gaussian distribution around the central point of laser focus, and when the critical fluctuations started to play a role, critical Casimir forces emerge and particles in traps start to feel external force aside from the optical forces and that external force causes a deviation

in Gaussian distribution of the particles in trap. This deviation from normal distribution, allows us to calculate how strong these forces are.

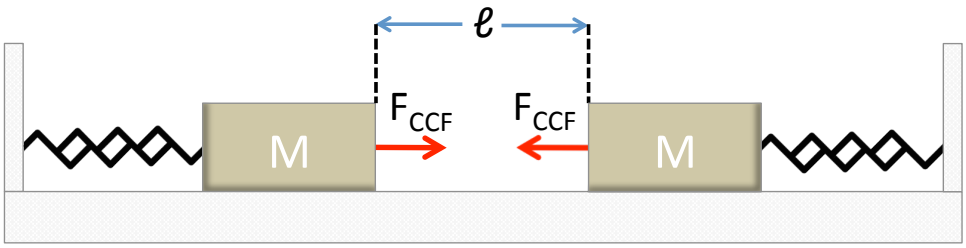

Figure 4.7: Spring mass analogy for the particle in an optical trap. *Representation of particles with mass m in optical traps with spring constant k. Here, F_{CCF} is the attractive critical Casimir forces acting on the system when the correlation length became comparable with the separation distance l between particles.*

First, we worked on the critical Casimir interaction between two bodies and for that, we have placed two colloids in the proximity of each other with the help of holgraphic optical tweezers. Then, the relative coordinate between particles were analysed in order to subtract common drift, noise due to pointing instability of laser or any other noisy effect that may be applied to both of the traps. This has been done by analysing the difference of the trajectories in both x and y directions.

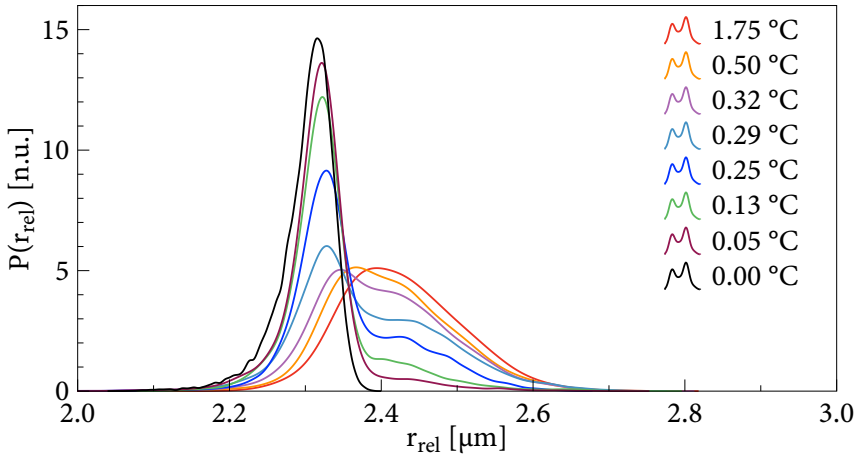

Figure 4.8: Probability distribution of relative coordinate with changing temperature. *Here, histogram of the differece of the trajectories were presented as a function of relative temperature to critical temperature ($T_C - T$).*

As the temperature getting closer to the critical point, correlation length(ξ) increases and give rise to critical Casimir forces. When $T_C - T \approx 0.5°C$, attractive force between particles become detectable and as $T_C - T$ getting closer to zero, magnitude of the forces become larger and the effect becomes more visible. Here, the trajectories which we developed the histograms from, show Kramer's transition like behaviour. In other words, while the temperature getting closer to the critical point, second potential were created aside from optical potential and when the potential become deep enough, particle starts to spend time in critical Casimir potential as well. The deeper critical Casimir potential, the more time particle spends inside. And finally, critical Casimir potential becomes so deep in a way that optical forces cannot beat the critical forces anymore and particles are stick to each other.

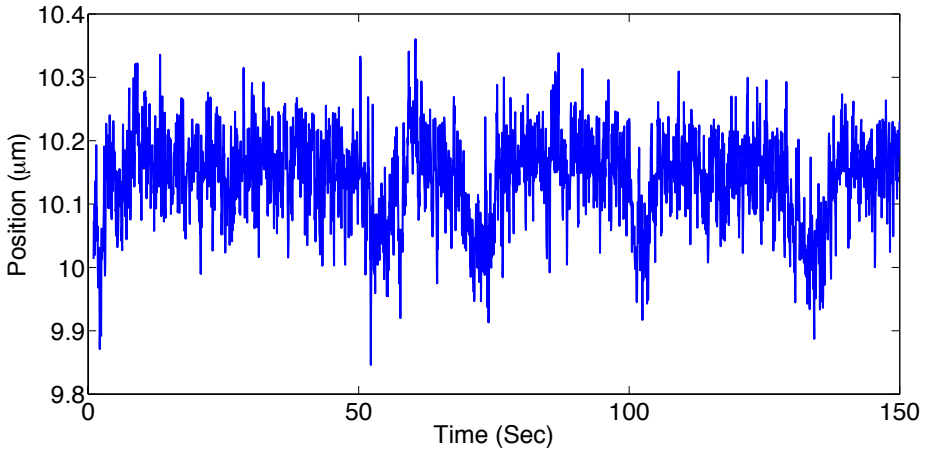

Figure 4.9: Kramer's transition like behaviour near critical point. *When* $(T_C - T)$ *is near zero, critical Casimir potential gets deeper and the particle shows Kramer's transition behaviour by jumping between optical and critical Casimir potentials.*

Besides the analysis of relative distance between particles, we have also investigated the correlation length(ξ) of the medium ($water - 2,6lutidine$) as a function of tempearature and the relative distance between particles changing with correlation length.

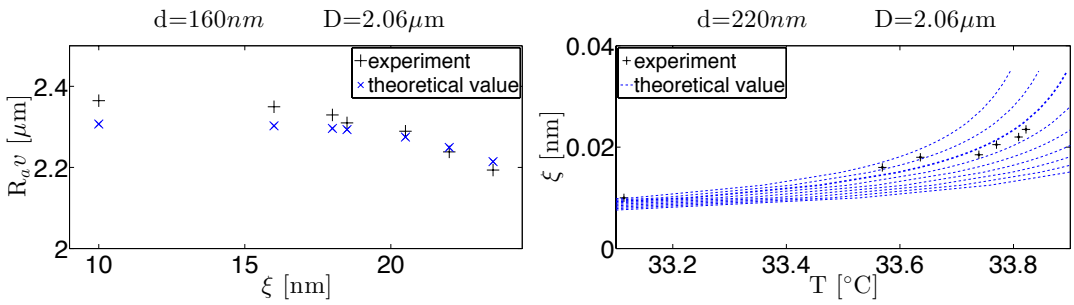

(a) **(b)**

Figure 4.10: Correlation length analysis. *Relative distance between particles were given as a function of correlation lenght(ξ) and evalution of ξ in temperature.*

4.4.2.1 Critical Casimir Forces Between 3 Particles

If the equations describing the forces are linear (like gravitational, magnetic or electrical forces), superpositon principle is applicable for addition of such forces. However, if nonlinearty is present, pairwise linear addition of forces is no longer valid and many-body effect comes into play. Many-body effect appear in variety of systems including nuclear matter[63], quantum-electro-dynamical Casimir forces[64, 65, 66], superconductivity[67], van der Waals forces amonng noble gases[68, 69] and colloidal suspensions[59, 70]. Many body effect for critical Casimir forces between 2 colloidal particles near a wall were studied theoretically[71] and here, we aimed to demonstrate experimentally the many-body effect for critical Casimir forces arises between 3 colloidal particles.

In order to observe the effect of the presence of the third body in the system, one needs to add the forces pairwise and the deviation from that result should give the many-body effect. For that, we have created an equilateral triangler shaped optical traps with identical (within 5% deviation) particles inside. Then, after the measurment of the interaction between two bodies, the third one get closer to the others and the interaction between the other two particles reinvestigated. If the net force between two colloids without any other interactions is assumned to be F, presence of the third particle should increase this force by a factor of $F/2$ to sum $3F/2$. Any deviation from that superpostion principle are assummed

to be the many-body effect.

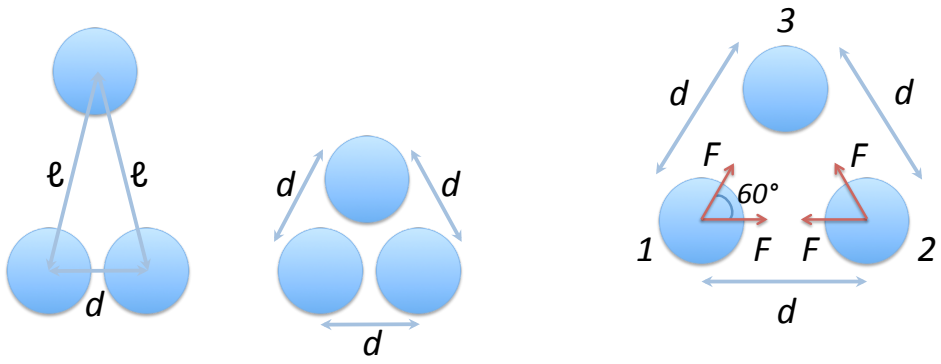

(a) **(b)**

Figure 4.11: Schematic of top view of different configurations used for the comparison of 2- and 3-body and force diagrams in action. *(a) $l \gg d$ so that the far particle doesnt have any effect on the others and so eligible for comparing with 3 body. (b) Total force acting on particle 1 is $2F$ and in lateral direction $3F/2$ if the forces are assumed to be pairwise additive.*

For the first measurement of such forces, we analysed the relative distance between particles 1 and 2 as denoted in Fig. 4.11 (b). And the results were compared with the 2 body measurements as shown in Fig. 4.11 (a). Surface-to-surface distance between 2 particles for both 2- and 3-body interactions are presented as a function of temperature in Fig. 4.12.

Here we observed that the presence of the third particle in the configuration clearly enhances the interaction between two particles. However, it is expected that the magnitude of enhancement is *1.5* if the forces are linearly additive like in electrostatic forces. However, the observed magnitude is $\approx$ *2* which considered to be the first sign of many body effect for the critical Casimir forces.

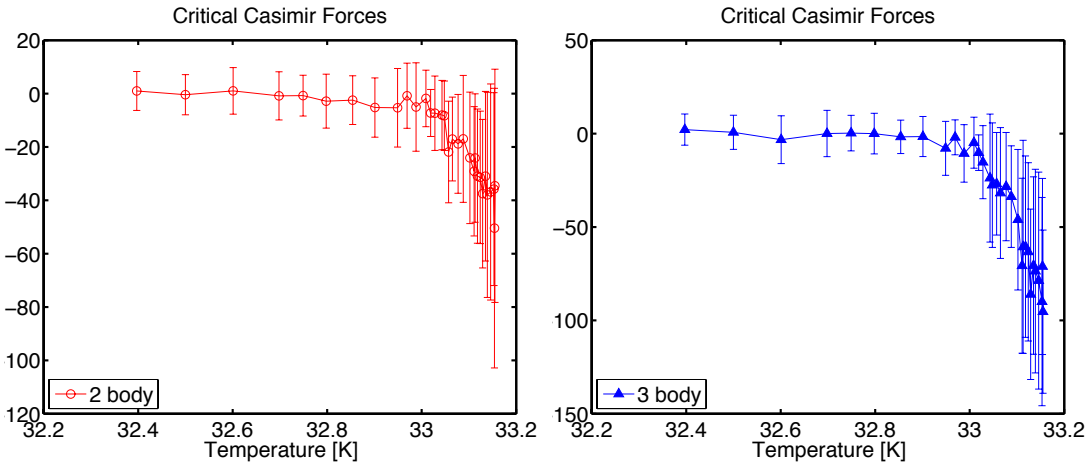

(a) **(b)**

Figure 4.12: Relative surface-to-surface distance between 2 particles without(a) and with(b) the third particle. *Presence of the third body in the system enhances the interaction between the other particles and this corresponds to an attractive critical Casimir interaction between 3 bodies.*

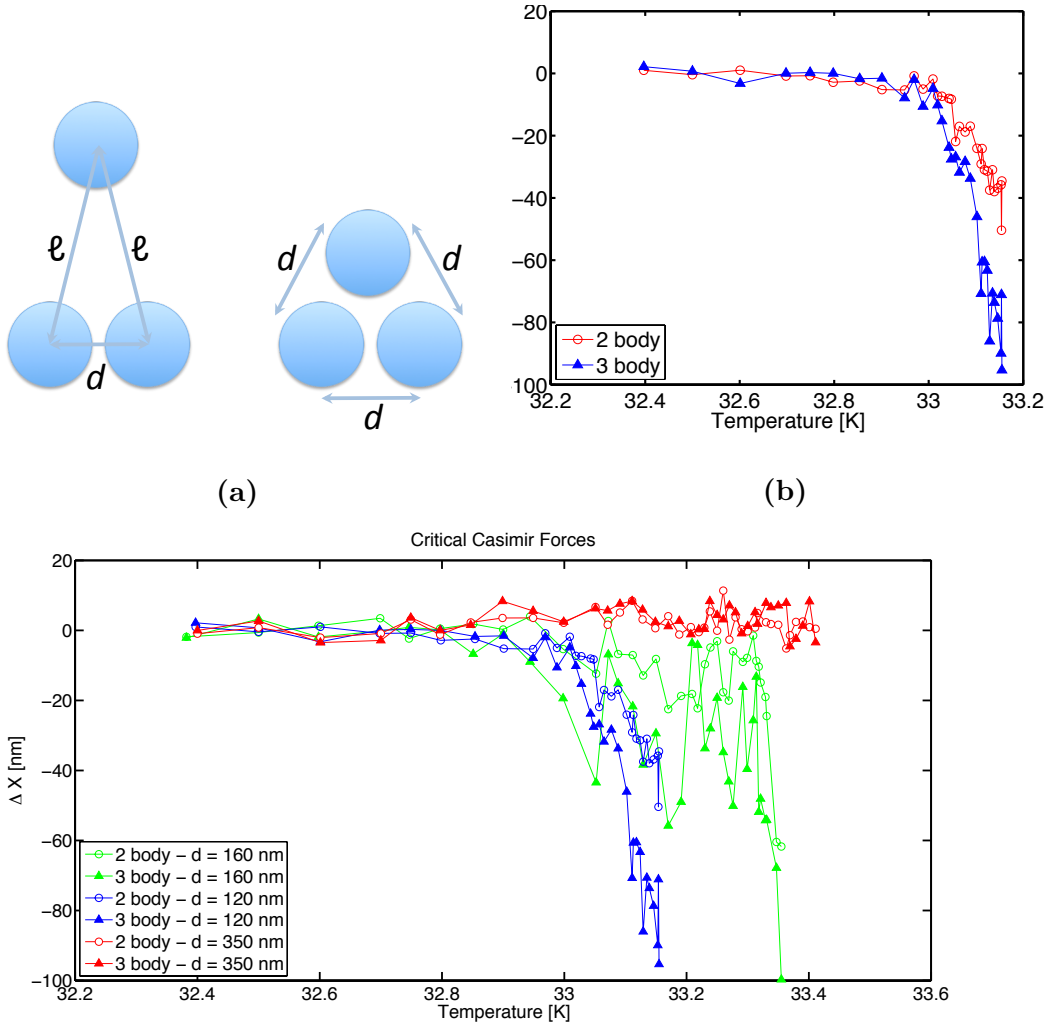

Figure 4.13: Comparison of relative surface-to-surface distances.(a) *Configurations to compare 2 and 3 body interactions.* (b) *Here the enhancement of the interaction due to the third body is* ≈ 1.33 *times larger than the expected value.* (c) *The same experiment is repeated with different surface-to-surface distances and the effect gets smaller and finally disappears.*

Chapter 5

Conclusion

Here, we explored novel aspects and applications of critical Casimir forces. Critical Casimir forces emerge between objects immersed in a binary liquid mixture kept near the critical point due to the confinement of the fluid density fluctuations. This effect has been recently demonstrated using total internal reflection microscopy (TIRM) for the case of a single spherical mesoscopic particle in front of a planar surface immersed in a critical mixture of walter and 2,6-lutidine[1]. The main advantage of critical Casimir forces is that they can be readily tuned by adjusting the criticality of the mixture[7, 9, 72, 73], and they can be made both attractive and repulsive[61, 74, 75]. In this project, we focused on the study of critical Casimir forces on particles in bulk[54], that have not been investigated experimentally before.

We started with the study of a single Brownian particle immersed in a critical mixture of water-2,6-lutidine, to elucidate how the critical fluctuations of the mixture couple to the intrinsic Brownian motion of the particle.

We proceeded with the study of critical Casimir forces between multiple objects. With this project we addressed the case of few particles and we tried to answers the questions of whether critical Casimir forces present three-body effects, how they are affected by hydrodynamic interactions and by the ineluctable presence of Brownian motion.

In details, we started with the case of two particles. We were able to see the mark of the electrostatic interaction in the distribution of the relative distance between the particles. We could see the effect of the critical Casimir fluctuations on the distribution of the relative distance between the particles, with the temperature approaching from below the critical temperature. We were able to reproduce numerically the observed behavior of the particle distance distribution.

Experimentally the main challenge was to control the temperature of the system to an accuracy of a few millikelvins.

Extending the knowledge about critical Casmir forces, one of the possible novel technological applications of the project is the possibility of using repulsive critical Casimir forces to prevent sticking between the metallic parts of nanodevices due to the presence of attractive QED Casimir forces. This is particularly relevant for future developments of nanotechnology.

Bibliography

[1] C. Hertlein, L. Helden, A. Gambassi, S. Dietrich, and C. Bechinger, "Direct measurement of critical casimir forces," *Nature*, vol. 451, pp. 172–175, 01 2008.

[2] A. Gambassi, "Critical casimir forces," *Internal Report*, 2014.

[3] A. Gambassi, "Relaxation phenomena at criticality," *The European Physical Journal B*, vol. 64, no. 3-4, pp. 379–386, 2008.

[4] M. Hasenbusch, "Thermodynamic casimir effect: Universality and corrections to scaling," *Phys. Rev. B*, vol. 85, p. 174421, May 2012.

[5] A. Gambassi, A. Maciołek, C. Hertlein, U. Nellen, L. Helden, C. Bechinger, and S. Dietrich, "Critical casimir effect in classical binary liquid mixtures," *Phys. Rev. E*, vol. 80, p. 061143, Dec 2009.

[6] M. E. Fisher and P. G. de Gennes, "Phenomena at the walls in a critical binary mixture," *C. R. Acad. Sci. Paris B*, vol. 287, no. 207, 1978.

[7] H. Casimir, "On the attraction between two perfectly conducting plates," *Proc. Koninklijke Nederlandse Akad. Wetenschappen B*, vol. 51, pp. 793–795, 1948.

[8] A. Gambassi, A. Maciołek, C. Hertlein, U. Nellen, L. Helden, C. Bechinger, and S. Dietrich, "Critical casimir effect in classical binary liquid mixtures," *Phys. Rev. E*, vol. 80, p. 061143, Dec 2009.

[9] U. Nellen, L. Helden, and C. Bechinger, "Tunability of critical casimir interactions by boundary conditions," *EPL (Europhysics Letters)*, vol. 88, no. 2, p. 26001, 2009.

[10] U. Nellen, J. Dietrich, L. Helden, S. Chodankar, K. Nygard, J. Friso van der Veen, and C. Bechinger, "Salt-induced changes of colloidal interactions in critical mixtures," *Soft Matter*, vol. 7, pp. 5360–5364, 2011.

[11] D. Bonn, J. Otwinowski, S. Sacanna, H. Guo, G. Wegdam, and P. Schall, "Direct observation of colloidal aggregation by critical casimir forces," *Phys. Rev. Lett.*, vol. 103, p. 156101, Oct 2009.

[12] G. Volpe, T. Brettschneider, L. Helden, and C. Bechinger, "Novel perspectives for the application of total internal reflection microscopy," *Opt. Express*, vol. 17, pp. 23975–23985, Dec 2009.

[13] L. P. Ghislain and W. W. Webb, "Scanning-force microscope based on an optical trap," *Opt. Lett.*, vol. 18, pp. 1678–1680, Oct 1993.

[14] J. C. Crocker and D. G. Grier, "Methods of digital video microscopy for colloidal studies," *Journal of Colloid and Interface Science*, vol. 179, no. 1, pp. 298 – 310, 1996.

[15] U. F. Keyser, J. van der Does, C. Dekker, and N. H. Dekker, "Optical tweezers for force measurements on dna in nanopores," *Review of Scientific Instruments*, vol. 77, no. 10, pp. –, 2006.

[16] O. M. Marago, P. H. Jones, P. G. Gucciardi, G. Volpe, and A. C. Ferrari, "Optical trapping and manipulation of nanostructures," *Nat Nano*, vol. 8, 2013.

[17] T. Brettschneider, G. Volpe, L. Helden, J. Wehr, and C. Bechinger, "Force measurement in the presence of brownian noise: Equilibrium-distribution method versus drift method," *Phys. Rev. E*, vol. 83, p. 041113, Apr 2011.

[18] G. Volpe, G. Volpe, and D. Petrov, "Brownian motion in a nonhomogeneous force field and photonic force microscope," *Phys. Rev. E*, vol. 76, p. 061118, Dec 2007.

[19] G. Volpe, R. Quidant, G. m. c. Badenes, and D. Petrov, "Surface plasmon radiation forces," *Phys. Rev. Lett.*, vol. 96, p. 238101, Jun 2006.

[20] J. Israelachvili, *Intermolecular and Surface Forces*. New York, USA: Academic Press, 1992.

[21] A. Gambassi and S. Dietrich, "Colloidal agregation and critical casimir forces," *Phys. Rev. Lett*, 2010.

[22] P. D. Gallagher and J. V. Maher, "Partitioning of polystyrene latex spheres in immiscible critical liquid mixtures," *Phys. Rev. A*, vol. 46, pp. 2012–2021, Aug 1992.

[23] B. M. Law, J.-M. Petit, and D. Beysens, "Adsorption-induced reversible colloidal aggregation," *Phys. Rev. E*, vol. 57, pp. 5782–5794, May 1998.

[24] J. H. Poynting, "On the transfer of energy in the electromagnetic field," *Philosophical Transactions of the Royal Society of London*, vol. 175, pp. 343–361, 1884.

[25] A. Ashkin, "Acceleration and trapping of particles by radiation pressure," *Phys. Rev. Lett.*, vol. 24, pp. 156–159, Jan 1970.

[26] A. Ashkin, J. M. Dziedzic, J. E. Bjorkholm, and S. Chu, "Observation of a single-beam gradient force optical trap for dielectric particles," *Opt. Lett.*, vol. 11, pp. 288–290, May 1986.

[27] A. Ashkin and J. Dziedzic, "Optical trapping and manipulation of viruses and bacteria," *Science*, vol. 235, no. 4795, pp. 1517–1520, 1987.

[28] D. N. Fuller, G. J. Gemmen, J. P. Rickgauer, A. Dupont, R. Millin, P. Recouvreux, and D. E. Smith, "A general method for manipulating dna sequences from any organism with optical tweezers," *Nucleic Acids Res.*, vol. 34, no. 2, p. e15, 2006.

[29] T. Uemura, H. Ohkura, Y. Adachi, K. Morino, K. Shiozaki, and M. Yanagida, "Dna topoisomerase ii is required for condensation and separation of mitotic chromosomes in s. pombe," *Cell*, vol. 50, no. 6, pp. 917–925, 2014.

[30] Y. Kimura and P. R. Bianco, "Single molecule studies of dna binding proteins using optical tweezers," *Analyst*, 2006.

[31] M. P. MacDonald, G. C. Spalding, and K. Dholakia, "Microfluidic sorting in an optical lattice," *Nature*, vol. 426, pp. 421–424, 11 2003.

[32] T. Bohlein, J. Mikhael, and C. Bechinger, "Observation of kinks and antikinks in colloidal monolayers driven across ordered surfaces," *Nat Mater*, vol. 11, pp. 126–130, 02 2012.

[33] S. Lin and K. B. Crozier, "Trapping-assisted sensing of particles and proteins using on-chip optical microcavities," *ACS Nano*, vol. 7, no. 2, pp. 1725–1730, 2013.

[34] Y. Tuna, R. Sayed, M. G. Donato, P. G. Gucciardi, O. Marago, and G. Volpe, "Optical feedback radiation forces: Intracavity optical trapping with feedback-locked diode lasers," in *Frontiers in Optics 2012/Laser Science XXVIII*, p. FTu4C.2, Optical Society of America, 2012.

[35] A. Ashkin, "Optical trapping and manipulation of neutral particles usinglasers," *Proceedings of the National Academy of Sciences*, vol. 94, no. 10, pp. 4853–4860, 1997.

[36] C. J. Foot, *Atomic Physics*. Oxford Univ. Press, 2005.

[37] T. wei Wu, J. Tang, B. Hajj, and M. Cui, "Phase resolved interferometric spectral modulation (prism) for ultrafast pulse measurement and compression," *Opt. Express*, vol. 19, pp. 12961–12968, Jul 2011.

[38] R. Bowman, N. Muller, X. Zambrana-Puyalto, O. Jedrkiewicz, P. Di Trapani, and M. Padgett, "Efficient generation of bessel beam arrays by means of an slm," *The European Physical Journal Special Topics*, vol. 199, no. 1, pp. 159–166, 2011.

[39] L. Gong, Y.-X. Ren, G.-S. Xue, Q.-C. Wang, J.-H. Zhou, M.-C. Zhong, Z.-Q. Wang, and Y.-M. Li, "Generation of nondiffracting bessel beam using digital micromirror device," *Appl. Opt.*, vol. 52, pp. 4566–4575, Jul 2013.

[40] D. G. Grier, "A revolution in optical manipulation," *Nature*, vol. 424, pp. 810–816, 08 2003.

[41] S. Tallieu, *Holographic optical trapping*. PhD thesis, Ghent University, June 2012.

[42] M. 7.14, "Introduction: Pid controller design," 2012.

[43] T. Wescott, *PID without PhD*. EE Times-India, October 2000.

[44] J. G. Ziegler and N. B. Nichols, "Optimum settings for automatic controllers," *Trans. ASME*, vol. 64, 1942.

[45] K. H. Ang, G. Chong, and Y. Li, "Pid control system analysis, design, and technology," *Control Systems Technology, IEEE Transactions on*, vol. 13, pp. 559–576, July 2005.

[46] I. Karatzas and S. Shreve, *Brownian Motion and Stochastic Calculus*. New York, USA: Springer, 1998.

[47] U. M. B. Marconi, A. Puglisi, L. Rondoni, and A. Vulpiani, "Fluctuationdissipation: Response theory in statistical physics," *Physics Reports*, vol. 461, no. 46, pp. 111 – 195, 2008.

[48] G. Volpe and G. Volpe, "Simulation of a brownian particle in an optical trap," *American Journal of Physics*, vol. 81, no. 3, pp. 224–230, 2013.

[49] R. Huang, I. Chavez, K. M. Taute, B. Lukic, S. Jeney, M. G. Raizen, and E.-L. Florin, "Direct observation of the full transition from ballistic to diffusive brownian motion in a liquid," *Nat Phys*, vol. 7, pp. 576–580, 07 2011.

[50] A. Rohrbach, "Switching and measuring a force of 25 femtonewtons with an optical trap," *Opt. Express*, vol. 13, pp. 9695–9701, Nov 2005.

[51] K. Berg-Srensen and H. Flyvbjerg, "Power spectrum analysis for optical tweezers," *Review of Scientific Instruments*, vol. 75, no. 3, pp. 594–612, 2004.

[52] G. Volpe and D. Petrov, "Torque detection using brownian fluctuations," *Phys. Rev. Lett.*, vol. 97, p. 210603, Nov 2006.

[53] T. F. Mohry, *Phase behavior of colloidal suspensions with critical solvents*. PhD thesis, Max-Planck-Institut fur Intelligente Systeme Institut fur Theoretische Physik IV, Universitat Stuttgart, February 2013.

[54] A. Hanke, F. Schlesener, E. Eisenriegler, and S. Dietrich, "Critical casimir forces between spherical particles in fluids," *Phys. Rev. Lett.*, vol. 81, pp. 1885–1888, Aug 1998.

[55] S. Kondrat, L. Harnau, and S. Dietrich, "Critical casimir interaction of ellipsoidal colloids with a planar wall," *The Journal of Chemical Physics*, vol. 131, no. 20, pp. –, 2009.

[56] A. Walther and A. H. E. Muller, "Janus particles," *Soft Matter*, vol. 4, pp. 663–668, 2008.

[57] R. Di Leonardo, J. Leach, H. Mushfique, J. M. Cooper, G. Ruocco, and M. J. Padgett, "Multipoint holographic optical velocimetry in microfluidic systems," *Phys. Rev. Lett.*, vol. 96, p. 134502, Apr 2006.

[58] E. R. Dufresne, T. M. Squires, M. P. Brenner, and D. G. Grier, "Hydrodynamic coupling of two brownian spheres to a planar surface," *Phys. Rev. Lett.*, vol. 85, pp. 3317–3320, Oct 2000.

[59] J. W. Merrill, S. K. Sainis, J. Blawzdziewicz, and E. R. Dufresne, "Many-body force and mobility measurements in colloidal systems," *Soft Matter*, vol. 6, pp. 2187–2192, 2010.

[60] J. Kotar, M. Leoni, B. Bassetti, M. C. Lagomarsino, and P. Cicuta, "Hydrodynamic synchronization of colloidal oscillators," *Proceedings of the National Academy of Sciences*, vol. 107, no. 17, pp. 7669–7673, 2010.

[61] D. Iannuzzi, M. Lisanti, and F. Capasso, "Effect of hydrogen-switchable mirrors on the casimir force," *Proceedings of the National Academy of Sciences*, vol. 101, no. 12, pp. 4019–4023, 2004.

[62] M. Trndle, O. Zvyagolskaya, A. Gambassi, D. Vogt, L. Harnau, C. Bechinger, and S. Dietrich, "Trapping colloids near chemical stripes via critical casimir forces," *Molecular Physics*, vol. 109, no. 7-10, pp. 1169–1185, 2011.

[63] T. Skyrme, "The effective nuclear potential," *Nuclear Physics*, vol. 9, no. 4, pp. 615 – 634, 19581959.

[64] A. Rodriguez, M. Ibanescu, D. Iannuzzi, F. Capasso, J. D. Joannopoulos, and S. G. Johnson, "Computation and visualization of casimir forces in arbitrary geometries: Nonmonotonic lateral-wall forces and the failure of proximity-force approximations," *Phys. Rev. Lett.*, vol. 99, p. 080401, Aug 2007.

[65] A. W. Rodriguez, A. P. McCauley, D. Woolf, F. Capasso, J. D. Joannopoulos, and S. G. Johnson, "Nontouching nanoparticle diclusters bound by repulsive and attractive casimir forces," *Phys. Rev. Lett.*, vol. 104, p. 160402, Apr 2010.

[66] S. J. Rahi, A. W. Rodriguez, T. Emig, R. L. Jaffe, S. G. Johnson, and M. Kardar, "Nonmonotonic effects of parallel sidewalls on casimir forces between cylinders," *Phys. Rev. A*, vol. 77, p. 030101, Mar 2008.

[67] L. P. Kadanoff and P. C. Martin, "Theory of many-particle systems. ii. superconductivity," *Phys. Rev.*, vol. 124, pp. 670–697, Nov 1961.

[68] J. A. Barker, "Many-body interactions in rare gases: Krypton and xenon," *Phys. Rev. Lett.*, vol. 57, pp. 230–233, Jul 1986.

[69] N. Jakse, J. M. Bomont, and J. L. Bretonnet, "Effects of three-body interactions on the structure and thermodynamics of liquid krypton," *The Journal of Chemical Physics*, vol. 116, no. 19, pp. 8504–8508, 2002.

[70] M. Brunner, J. Dobnikar, H.-H. von Grünberg, and C. Bechinger, "Direct measurement of three-body interactions amongst charged colloids," *Phys. Rev. Lett.*, vol. 92, p. 078301, Feb 2004.

[71] T. G. Mattos, L. Harnau, and S. Dietrich, "Many-body effects for critical casimir forces," *The Journal of Chemical Physics*, vol. 138, no. 7, pp. –, 2013.

[72] R. J. L. Andon and J. D. Cox, "896. phase relationships in the pyridine series. part i. the miscibility of some pyridine homologues with water," *J. Chem. Soc.*, pp. 4601–4606, 1952.

[73] J. D. Cox and E. F. G. Herington, "The coexistence curve in liquid-liquid binary systems," *Trans. Faraday Soc.*, vol. 52, pp. 926–930, 1956.

[74] F. Capasso, J. Munday, D. Iannuzzi, and H. B. Chan, "Casimir forces and quantum electrodynamical torques: Physics and nanomechanics," *Selected Topics in Quantum Electronics, IEEE Journal of*, vol. 13, pp. 400–414, March 2007.

[75] J. N. Munday, F. Capasso, and V. A. Parsegian, "Measured long-range repulsive casimir-lifshitz forces," *Nature*, vol. 457, pp. 170–173, 01 2009.

Appendix A

Code

A.1 Tracking Code

```
%% INITIALIZATION
clear all; close all; clc;

%% TRACKING SETTINGS
FigNumber = 0;
Fig2Number = FigNumber;
ErodeRadius = 1;          % size of the structure element for erosion,
%diameter = 2*erodeRadius + 1
DilateRadius = 1;         % size of the structure element for the
%following dilation, diameter = 2*dilateRadius + 1
MinParticleRadius = 2;    % important for size filtering
MaxParticleRadius = 15;

%% Get number of files in directory
FilePath = uigetdir('D:\Experiment\SLM\Data');
FileAppendix = '\';
FilePath = strcat(FilePath,FileAppendix);
listing = dir(fullfile(FilePath));
TotalNumberOfFiles = numel(listing)
```

```
Temp = zeros(TotalNumberOfFiles-2,12);

%% Analyze all Videos in the folder
A_MeanDistance = zeros(TotalNumberOfFiles-2,1)

for FileNumber = 3:1:TotalNumberOfFiles %We start at 3 because the
%first 2 files are listed as '.' and '..'
     %% Run the analyzing code

        %% CHOOSING FILE
        FileName = listing(FileNumber).('name');

        %% LOAD VIDEO
        Video = VideoReader([FilePath FileName]);
        NumberOfFrames = Video.NumberOfFrames;
        Tracking.FrameRate = Video.FrameRate;

        tic %for the tictoc-function that measures the elapsed time
        %between tic and toc in the code

        for i = 1:1:NumberOfFrames
%             disp(['** TRACKING (' FileName ')- frame ' int2str(i) '/'...
%                int2str(NumberOfFrames) ' - ' int2str(toc) '.' ...
%                  int2str(mod(toc,1)*10) 's']);

            VideoPortion = read(Video,i);

            ImageRaw = mean(VideoPortion,3); % reduce to 8 bit

            ImageMask = ImageRaw > 70 ; % create mask at desired cut off level
 %          ImageMask(10:390,10:350) = ImageRaw(10:390,10:350) <20 ;
            % create mask at desired cut off level
            ImageErode = imerode(ImageMask,ErodeRadius); % erode
            ImageOpen = imdilate(ImageErode,DilateRadius); % dilate

            [Regions,NumberOfRegions] = bwlabel(ImageOpen,8); % label particle
            %regions, get number of detected regions
            Props = regionprops(Regions, 'Centroid', 'Area'); % get coordinates
            %and sizes for all particles
```

```
X = [];
Y = [];
for n = 1:1:NumberOfRegions; % analyze particles in frame
    SizeOfRegion = Props(n).Area;
    if  (pi*(MinParticleRadius+DilateRadius-...
        ErodeRadius)^2<SizeOfRegion && ...
            SizeOfRegion<pi*(MaxParticleRadius+...
                DilateRadius-ErodeRadius)^2);
        X = [X;Props(n).Centroid(1)];
        Y = [Y;Props(n).Centroid(2)];
    end
end
Tracking.Position(i).X = X;
Tracking.Position(i).Y = Y;

if (FigNumber>0)
    figure(FigNumber)

    subplot(2,1,1)
    imagesc(ImageRaw)
    hold on
    plot(X,Y,'or','MarkerSize',8)
    text(50,50,[FileName ' - Frame ' int2str(i)...
         '/' int2str(NumberOfFrames)],...
        'Color','k','BackgroundColor',[1 1 1],'Interpreter','none')
    hold off
    axis equal
    colormap bone
    xlabel('Pixels')
    ylabel('Pixels')

    subplot(2,1,2)
    imagesc(ImageMask)
    hold on
    plot(X,Y,'or','MarkerSize',8)
    text(50,50,[FileName ' - Frame ' int2str(i)...
         '/' int2str(NumberOfFrames)],...
        'Color','k','BackgroundColor',[1 1 1],'Interpreter','none')
    hold off
    axis equal
```

```
        colormap bone
        xlabel('Pixels')
        ylabel('Pixels')

    end
end

%% TRACES
Trace.X1 = [];
Trace.Y1 = [];
Trace.X2 = [];
Trace.Y2 = [];
for i = 2:1:length(Tracking.Position)
    Trace.X1 = [Trace.X1 Tracking.Position(i).X(1)];
    Trace.Y1 = [Trace.Y1 Tracking.Position(i).Y(1)];
    Trace.X2 = [Trace.X2 Tracking.Position(i).X(2)];
    Trace.Y2 = [Trace.Y2 Tracking.Position(i).Y(2)];
end

if (FigNumber>0)
    figure(FigNumber)

    subplot(2,2,3)
    hold on
    plot(Trace.X1,Trace.Y1,'r')
    hold off
    axis equal
    xlabel('Pixels')
    ylabel('Pixels')
end

%% TRAJECTORIES
Pixel2MicronsX = 0.08873; % Conversion factor from pixels to um
Pixel2MicronsY = 0.08873; % Conversion factor from pixels to um
FrameRate = Video.FrameRate;

%T = [1:1:length(Trace.X1)]/FrameRate;
Trajectory.X1 = Trace.X1*Pixel2MicronsX;
Trajectory.Y1 = Trace.Y1*Pixel2MicronsY;
Trajectory.X2 = Trace.X2*Pixel2MicronsX;
```

```
        Trajectory.Y2 = Trace.Y2*Pixel2MicronsY;

        %% ANALYSIS
        %Save Trajectory Parameters:
        AllTrajectories(FileNumber-2,1) = Trajectory; %adds current Trajectory
        %to the overall set of all Trajectories
        %Save NumberOfFrames Parameters:
        AllFrames(FileNumber-2,1) = NumberOfFrames;
        %Save FrameRate Parameters:
        AllFrameRates(FileNumber-2,1) = Video.FrameRate;
        %Save ImageRaw Parameters:
        SingleImageRaw.Img = ImageRaw; %Create Structure for putting
        %Image-matrix into a 1x1 structure field
        AllImageRaws(FileNumber-2,1) = SingleImageRaw; %Put these structure
        %fields into a new vector for later use

        % Get MeanDistance for the Distance(T)-Function-Plot
        Temp(FileNumber-2,1:length(FileName)-6) = double(FileName(1:end-6));
        % Convert Temperatures for plot

        DistanceSphereThreeOne(FileNumber-2) = sqrt((mean(Trajectory.X1)-...
            mean(Trajectory.X2))^2+(mean(Trajectory.Y1)-mean(Trajectory.Y2))^2)

    Temp = char(Temp)

%% Plot Histogram
    T_plot = str2num(Temp(:,1:6));
    plot(T_plot, DistanceSphereThreeOne)

% Save the matlab files
    save(chat(2,FilePath(1:end-5),'MatlabFiles.mat'))
```